HEART SOUND SEGMENTATION USING SIGNAL PROCESSING METHODS

A THESIS SUBMITTED TO
THE GRADUATE SCHOOL OF ENGINEERING AND SCIENCE
OF BILKENT UNIVERSITY
IN PARTIAL FULFILLMENT OF THE REQUIREMENTS FOR
THE DEGREE OF
MASTER OF SCIENCE
IN
COMPUTER ENGINEERING

By
Devrim Şahin
July, 2015

HEART SOUND SEGMENTATION USING SIGNAL PROCESSING METHODS
By Devrim Şahin
July, 2015

We certify that we have read this thesis and that in our opinion it is fully adequate, in scope and in quality, as a thesis for the degree of Master of Science.

Assoc. Prof. Dr. Hakan Ferhatosmanoğlu (Advisor)

Assoc. Prof. Dr. Çiğdem Gündüz Demir

Assist. Prof. Dr. Aybar C. Acar

Approved for the Graduate School of Engineering and Science:

Prof. Dr. Levent Onural
Director of the Graduate School

ABSTRACT

HEART SOUND SEGMENTATION USING SIGNAL PROCESSING METHODS

Devrim Şahin
M.S. in Computer Engineering
Advisor: Assoc. Prof. Dr. Hakan Ferhatosmanoğlu
July, 2015

Heart murmurs are pathological heart sounds that originate from blood flowing with abnormal turbulence due to physiological defects of the heart, and are the prime indicator of many heart-related diseases. Murmurs can be diagnosed via auscultation; that is, by listening with a stethoscope. However, manual detection and classification of murmur requires clinical expertise and is highly prone to misclassification. Although automated classification algorithms exist for this purpose; they heavily depend on feature extraction from 'segmented' heart sound waveforms. Segmentation in this context refers to detecting and splitting cardiac cycles. However, heart sound signal is not a stationary signal; and typically has a low signal-to-noise ratio, which makes it very difficult to segment using no external information but the signal itself. Most of the commercial systems require an external electrocardiography (ECG) signal to determine S_1 and S_2 peaks, but ECG is not as widely available as stethoscopes. Although algorithms that provide segmentation using sound alone exist, a proper comparison between these algorithms on a common dataset is missing. We propose several modifications to many of these algorithms, as well as an evaluation method that allows a unified comparison of all these approaches. We have tested each combination of algorithms on a real data set [1], which also provides manual annotations as ground truth. We also propose an ensemble of several methods, and a heuristic for which algorithm's output to use. Whereas tested algorithms report up to 62% accuracy, our ensemble method reports a 75% success rate. Finally, we created a tool named UpBeat to enable manual segmentation of heart sounds, and construction of a ground truth dataset. UpBeat is a starting medium for auscultation segmentation, time-domain based feature extraction and evaluation; which has automatic segmentation capabilities, as well as a minimalistic drag-and-drop interface which allows manual annotation of S_1 and S_2 peaks.

Keywords: Heart sound, Segmentation, Fourier, Wavelet transform.

ÖZET

İŞARET İŞLEME YÖNTEMLERİ KULLANILARAK KALP SESİ BÖLÜTLEME

Devrim Şahin
Bilgisayar Mühendisliği, Yüksek Lisans
Tez Danışmanı: Assoc. Prof. Dr. Hakan Ferhatosmanoğlu
Temmuz, 2015

Kalpte oluşan fiziksel bozuklukların kan akışını etkilemesi sonucu oluşan seslere üfürüm denir. Üfürümler birçok kalp hastalığının birincil habercisidir. Kalp seslerini stetoskop aracılığıyla dinlemek (oskültasyon) suretiyle üfürümler üzerinden teşhis yapılabilse de, bu tür teşhisler tıbbi uzmanlık gerektirmektedir ve hatalara oldukça açıktır. Literatürde otomatik sınıflandırma algoritmaları önerilmiş olsa da; ses dalgabiçimlerinden ayıklanacak olan özniteliklerin kalp atımı içerisindeki konumları teşhis açısından önem taşıdığı için, öncelikle birinci ve ikinci kalp seslerinin konumlarını belirlemek ve buna göre öznitelik seçmek gereklidir. Kalp atımlarının saptanması ve ayrıştırılması işlemine bölütleme (segmentasyon) adı verilmektedir. Kalp sinyalinin organik yapısı dolayısıyla öngörülebilir bir frekans-zaman profilinin olmaması, sadece ses kaydını kullanarak bölütleme işini zorlaştırmaktadır. Birçok ticari sistemde harici olarak bir elektrokardiyografi (EKG) sinyali de kaydedilse de, EKG aygıtlarının stetoskop kadar yaygın olmaması bu sistemlerin erişilebilirliğini düşürmektedir. Yalnızca kalp sesi kullanarak bölütleme yapan algoritmalar olsa da, bu algoritmaların hepsinin üzerinde sonuç sunduğu ortak bir veritabanı yoktur. Bu çalışmada, var olan algoritmalara çeşitli uyarlamaların yanı sıra, bu çeşitlemeleri karşılaştırmak için kullanılabilecek bir değerlendirme ölçütü öneriyoruz. Örnekleri için elle yapılmış bölütlemelerin mevcut olduğu Pascal [1] veritabanından alınmış 66 kayıt üzerinde bu yaklaşımların tüm kombinasyonlarını karşılaştırıyoruz. Bunun yanı sıra birkaç yöntemi karıştırarak sonuç kalitesini artırmayı amaçlayan bir birleşim de öneriyoruz. Karşılaştırdığımız tekil algoritmalar %62'ye varan başarılar gösterirken önerdiğimiz birleşim ile %75'lik bir başarı oranına ulaştık. Son olarak, Pascal gibi denetleme amaçlı veritabanlarının kolayca ve hatasız şekilde oluşturulabilmesi için bir araç ürettik.

Anahtar sözcükler: Kalp sesi, Bölütleme, Fourier, Dalgacık dönüşümü.

Acknowledgement

"Think where man's glory most begins and ends, and say my glory was I had such friends."

—William Butler Yeats

Of all the people I have met in my life, the two very best are the two very first. Mom, dad; you are absolutely irreplaceable to me. Thank you for being exceptionally amazing parents, I am proud to be your child.

My supervisor and role model, Prof. Dr. Hakan Ferhatosmanoğlu; thank you for your endless patience, wisdom, support; and the sense of direction you have provided me whenever I felt devoid of purpose.

I thank every teacher and mentor of mine with endless gratitude for their selflessness. Especially Fikret Ekin, Banu Özdemir, Metin Tiraki, Sedat Kayak, Hürriyet Yıldız and İnci Yıldız; I owe you my endless passion for knowledge. You will always be the moons on a bright sky by which I find my path.

All my precious friends (whom I cannot thank one by one, for I have many); thank you for being there for me. If I have ever made any you happy in return, then mine is a life well spent. Musa Tunç Arslan; your absence would hurt.

Coffee mugs and teapots of the world; whatever I did, you have always been by my side. I love you unconditionally.

So long, and thanks for all the fish.

(This study is financially supported by TÜBİTAK National Scholarship Programme for MSc Students.)

Contents

List of Figures

List of Tables

Chapter 1

Introduction

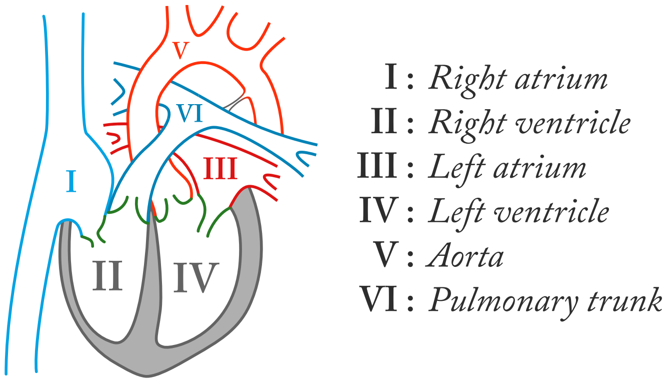

Figure 1.1: The anatomy of mammal heart

In living organisms, distribution and transportation of blood is conducted by the *cardiovascular system*. The circulation of blood allows the cardiovascular system to transport oxygen to and carbon dioxide from cells; distribute nutrients, hormones, blood cells; as well as fight pathogens, regulate acidity, body temperature, glucose concentration etc. [2]

Cardiovascular system consists of the heart, blood and blood vessels [3]. Heart is the central component of the circulatory system. It pumps oxygenated blood into the cells and collects oxygen-poor blood to the lungs. Correct operation of the heart is, thus, vitally important. Among the 57 million deaths that occurred globally in 2008, 36 million were due to non-communicable diseases (NCDs), of which the most common is cardiovascular diseases [4]. Turkey's profile in fighting heart diseases is not promising either; where NCDs are accounted for approximately 86% of total deaths, the highest of which is cardiovascular diseases with a proportion of 47% [5]. This makes detection and classification of heart diseases very important.

Figure 1.1 depicts the mammal heart. The left and right sides of the heart are isolated from each other; and perform slightly different tasks simultaneously. Each side is divided into two chambers with a valve in between. The smaller chambers that are on top are named the *atria*, whereas the lower chambers are called *ventricula* [6]. The blood enters the heart through the atria on both sides; the right side receives oxygen-poor blood collected from the body, whereas the left-side receives oxygen-rich blood collected from the lungs. When both atriums contract, the blood is pumped into the ventricles on both sides. After this, the ventricular muscles contract strongly and pump the blood into the pulmonary trunk on the right, which carries oxygen-poor blood into the lungs; and aorta on the left, which distributes oxygen-rich blood to the body. During these two contractions, two audible sounds are generated, called 'lub' and 'dub' respectively. There exist four valves in between these chambers which prevent blood from leaking backwards during each of the contractions. [2]

Heart is a complicated machinery that may fail to operate correctly on many levels. Putting severe cases as traumatic ruptures and heart attacks aside, anatomical or developmental defects can occur. One example is the failure of heart valves to properly close, in which case some of the blood flows backwards turbulently. Another problem may occur in the thin blood vessel named Ductus Arteriosus between the pulmonary artery and aorta (depicted in Figure 1.1). This vessel is used in fetuses to bypass the lungs that are not yet functional, but closes in birth and becomes the arterial ligament. However, a failure in the developmental stage can cause this vessel to remain open, leading to the congenital disorder known as Patent Ductus Arteriosus (PDA), causing shortness of breath and poor growth etc. [7] Both of these problems present themselves with a characteristic abnormal sound, known as a *heart murmur*.

There are various tools and techniques available for cardiologists to achieve a diagnosis, including auscultation, electrocardiography, echocardiography, Holter monitors, computer tomography, magnetic resonance imaging and so on. However, most of these options require an expensive setup. For example, magnetic resonance imaging (MRI) requires a medical MRI scanner, which has a cost of more than $1000 *per scan* (United States national median cost, excluding insurance) [8]. In Turkey, the price the patient is to pay is as low as 72 TRY [9], but the rest of the expense is then covered by the state. In any case, this prevents medical doctors from asking for an MRI scan immediately for every patient. Therefore, even when cardiologists suspect that a more complicated test is required, they decide to resort to simpler, less expensive methods as a first step. The simplest, cheapest, and therefore most commonly used technique is known as *cardiac auscultation*.

Cardiac auscultation (or "auscultation", shortly) is the process of listening to heart sounds using a simple equipment such as a stethoscope. If these heart sounds are recorded, the recording is called a *phonocardiogram*, or *PCG*. As a medical test, auscultation is fairly simple to apply; and the only required equipment being the stethoscope, it is virtually cost-free. This means that even in third-world countries, auscultation has a very broad availability.

The problem with auscultation, however, is that the interpretation of the sounds heard (or recorded) is not trivial. Diagnosis through cardiac auscultation requires years of clinical expertise and proper education to conduct properly. Furthermore, even with years of experience, the analysis remains critically subjective. It is reported that up to 80% of diagnoses made by expert physicians using auscultation are actually incorrect [10]. The main reason the error rates are as high as reported is that auscultatory analysis is very inconclusive. Since the well-being of the patients is involved, physicians tend to make Type-I errors (false alarms) almost deliberately, in order to avoid missing any potential abnormalities. This is a necessary attitude when the cost of Type-II errors (misses) is high (*e.g.* advancement of diseases, possibly death).

Given that auscultation is a comparably inconclusive test, one can argue that increasing the reliability of the test by developing an objective auscultation analysis approach would allow the physicians to avoid a significant amount of expense, creating a relief on the healthcare budgets of especially less developed countries [10]. Such a system would then increase the confidence of the diagnosis, and thus broaden availability of cardiac diagnostics even where more complicated tests are not easily accessible. With the electronic stethoscopes becoming more available by the day, it is now possible to discuss the possibility of an computer-aided affordable analysis tool that will provide objective measures of heart disease risks.

There have been numerous approaches for detecting heart diseases using a range of signal processing and machine learning techniques. The majority of these algorithms share a three-step approach; involving (1) cardiac cycle segmentation, (2) feature extraction, and (3) classification. The last two steps are well-studied in the literature; many different machine learning approaches including but not limited to support vector machines, artificial neural networks, even decision trees were applied on the problem of the classification of heart sounds once they are segmented [6, 10–26], however the approaches to the segmentation step remain outdated. Bentley et al. acknowledge that once the segmentation challenge is solved, the following steps will be "considerably easier"[1].

Cardiac cycle segmentation (the details of which will be discussed in length) is detection of the 'beats' of heart, such that any abnormalities determined can be taken into consideration regarding its location. Location of an abnormal component in the phonocardiogram is a very important feature for classification of *heart murmurs*. Murmurs are one of the most common abnormalities that can be detected via auscultation. These are audible turbulent sounds which may be generated by leaking heart valves, holes in cardiac muscles, developmental disorders, and a myriad of other conditions [7]. For all of these cases, the characteristics of the murmur change drastically. Murmurs can appear at different locations in the cardiac cycle, may increase or decrease in amplitude, be constantly loud; or may be observed at different frequency bands and different auscultation locations. All of these features help detecting the nature of the murmur.

However, trying to find the characteristics of murmur using only one cardiac cycle is not a reliable approach. Heart sound recordings are rarely (if ever) devoid of noise; moreover, the statistical properties of the noise present in such signals remain to be unpredictable: Additive white noise, lung sounds, mechanical sounds, loud peaks originating from physical movement of the stethoscope, even reverberations of the original heart sound echoing from internal tissues frequently appear in the phonocardiogram. Hence, it is critical to have a robust segmentation algorithm that is capable of correctly detecting as many cardiac cycles as possible in order to make reliable diagnoses.

In this study, we investigate several approaches to heart sound segmentation using only phonocardiogram recordings. The initial approach is a six-step algorithm, of which majority of the work in the literature is a variation [6, 11, 13, 15–19, 23, 25, 27–32]. These six steps include preprocessing (resampling and normalization), a time-frequency transform (selection of relevant frequency bands), rectification (transformation of the signal to a non-negative domain that represents magnitude), envelope detection (elimination of high frequency modulation), peak selection (thresholding and detection of peak candidates), and peak merging (elimination of redundant peaks and classification of the remaining candidates as S_1/S_2). Throughout the literature, different studies have proposed different methods for each of these six steps. We provide a comparison of these works by implementing all of these variations and testing every combination on a common real data set [1]. As a contribution, we also propose a modified version of the Maximal Marginal Relevance (MMR) method [33], which is widely used in the information retrieval context, as an alternative to the traditional approach. We define the similarity metrics that MMR uses such that diverse peaks are picked, maximizing both their amplitudes and temporal distances to each other. We also introduce an ensemble of the aforementioned methods in order to boost the algorithm's performance. For our tests, we use the annotated Pascal heart sound data set [1] and score each algorithm using a common evaluation metric that we propose. Finally, we developed an application that helps constructing and annotating a ground truth data set for heart sound segmentation, which is also a powerful tool for waveform visualization and playback, useful in providing an intuition for cardiac auscultation.

The rest of this thesis is organized as follows:

Chapter 2 provides a mathematical background for the signal processing techniques required for the discussion of our work.

Chapter 3 formally presents the problem, challenges and limitations; and summarizes the methodology and results of the related work in cardiac cycle segmentation.

Chapter 4 introduces UpBeat, a heart sound signal visualization, playback and annotation tool that we have developed.

Chapter 5 discusses the implementation of the heart sound segmentation algorithms in detail.

Chapter 6 explains the dataset, introduces our evaluation metric; then lists and discusses the results for both individual methods and the ensemble. Finally we conclude by discussing future work.

Chapter 2

Mathematical Background

In this section we will describe most of the approaches taken in the related work and this study. Although topics such as Fourier Transform are mentioned for the sake of completeness, a certain level of knowledge of signal processing is assumed with the intent of keeping the discussion brief and to-the-point.

2.1 Time-Frequency Transforms

Since a heart sound recording consists of both relevant and irrelevant information of different frequencies, it is a common practice to perform a time-frequency transform on the initial heart sound signal in order to filter and de-noise the original signal. Several time-frequency transform methods are discussed below, after a brief discussion of the Fourier transform.

2.1.1 Fourier Transform

Fourier transform is an operation that matches a signal onto the orthogonal Fourier space [34]. What it accomplishes is representing a time-domain signal in terms of a summation of its weighted sinusoidal components with different frequencies. As a result it provides a frequency domain representation of the signal. It is formulated in the continuous domain as follows [35]:

$$F(k) = \frac{1}{2\pi} \int_{-\infty}^{\infty} f(x) e^{-ikx} dx$$

Reverse Fourier transform is defined as the inverse of this operation, where the frequency domain representation of the signal is converted to a time frequency signal:

$$f(x) = \frac{1}{2\pi} \int_{-\infty}^{\infty} F(k) e^{ikx} dk$$

Discrete Fourier Transform (DFT) is defined on a discrete series $x[n]$ as below:

$$F[k] = \sum_{j=0}^{N-1} x[k] e^{-i2\pi jk/N}$$

Both the input and the output of the Fourier transform are complex, therefore are difficult to imagine. Converting the complex number z to its amplitude-phase notation is often more meaningful:

$$z = a + ib \implies |z| = \sqrt{a^2 + b^2}, \qquad \angle z = arctan(\frac{b}{a}).$$

Then $z = |z|e^{i\angle z}$. This is the radial notation of a complex number z on the complex domain, where $|z|$ is the amplitude and $\angle z$ is the positive angle to the real axis. While the amplitude of the Fourier transform of a signal ($|F(k)|$) represents the 'amount' of every frequency in the given signal, phase of the Fourier transform ($\angle F(k)$) keeps the phase information (or 'time delay', indirectly) for each frequency k. Every plot of a Fourier transform in this thesis will depict the amplitude of the transform only. Since we are interested in the amount in each frequency instead of the phase of it, this intuitively makes sense. However we keep both real and imaginary values separately in the code.

To further simplify the matters, we will use the property that if the input of the

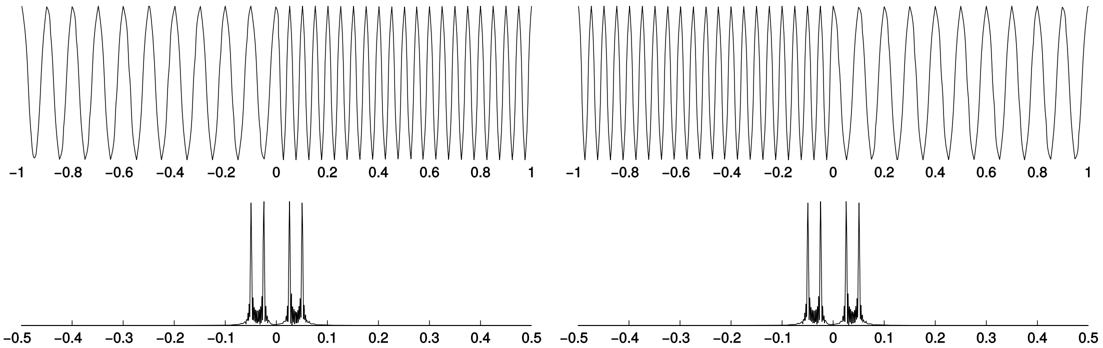

Figure 2.1: On the left is $f_1(t)$ and its Fourier transform. On the right is $f_2(t)$ and its Fourier transform. The amplitudes on the frequency domain are identical.

Fourier transform is strictly real, the output is symmetrical along the y-axis, that is; $F(k) = F(-k)$ iff $\Re\{f(x)\} = f(x)$. For our application, it is a given that the recorded data is real. Therefore it is possible to consider only positive frequencies for a real input, since the negative side will be redundant.

2.1.2 Short-Time Fourier Transform and Spectrogram

Fourier transform is informative for signals where the frequency distribution of the signal does not change significantly. For other signals where there the frequencies that the signal consists of, or their amplitudes change; the result will become a superposition of them. Consider two signals as follows: In the first signal, we have $f_1(t) = u(-t)cos(2\pi 10t) + u(t)cos(2\pi 20t)$, where $u(t)$ is the step function. This signal is a cosine with a $10Hz$ frequency up to $t = 0$, then changes its frequency into $20Hz$. Also let $f_2(t) = u(t)cos(2\pi 10t) + u(-t)cos(2\pi 20t)$, that is, the frequency drops from $20Hz$ to $10Hz$ at $t = 0$. The Fourier transforms of these two signals $F_1(k)$ and $F_2(k)$ are equivalent, in that $|F_1(k)| = |F_2(k)|$ (see Figure 2.1). Therefore it is said that Fourier transform loses the time information.

For many applications, we want to keep the time information; that is, we have a signal of which the frequency distribution is dynamic and should be attributed to time itself. That is to say, we would like to find out which frequencies are present at which time. One example to this is finding the notes of a song: Finding which notes are present in the song is never enough, we also would like to know their locations in time to analyse a song. Therefore we need a function that maps a time-domain signal onto the time-frequency domain.

One way of doing this is separating the signal to small time periods, then taking the Fourier transform for each period. This approach is called STFT (Short-Time Fourier Transform) [36]:

$$STFT_{x[n]}(m, f) = \sum_{n=-\infty}^{\infty} x[n]w[n-m]e^{-i2\pi fn}$$

Here, $w[n]$ is a window function (such as a Hann window) that helps reduce artifacts. Although this approach is intuitive, one disadvantage is that there exists a trade-off between frequency and time *resolutions*. When we keep the time periods very small, very quick changes in frequency can be detected precisely, however the frequencies themselves cannot be clearly detected (because each Fourier transform has small number of samples to work on). If we keep the intervals too large, the frequency resolution increases, however detecting the position of the frequency change exactly becomes a problem. Another approach to transforming the signal onto the time-frequency domain is known as wavelet transform.

Finally, spectrogram is defined as the squared magnitude of the Short-Time Fourier Transform; that is, $|STFT(t, w)|^2$.

2.1.3 Wavelet Transform

Wavelet transform is another method of representing a function in the form of a given orthonormal basis function. Whereas Fourier transform loses the time information altogether, wavelets are capable of representing both time and frequency axes with different resolutions [37].

Wavelet transform differs from Short-Time Fourier Transform on how it samples from the time-frequency domain. While STFT divides the time-frequency domain into equal time and frequency intervals as a grid; wavelet transform follows

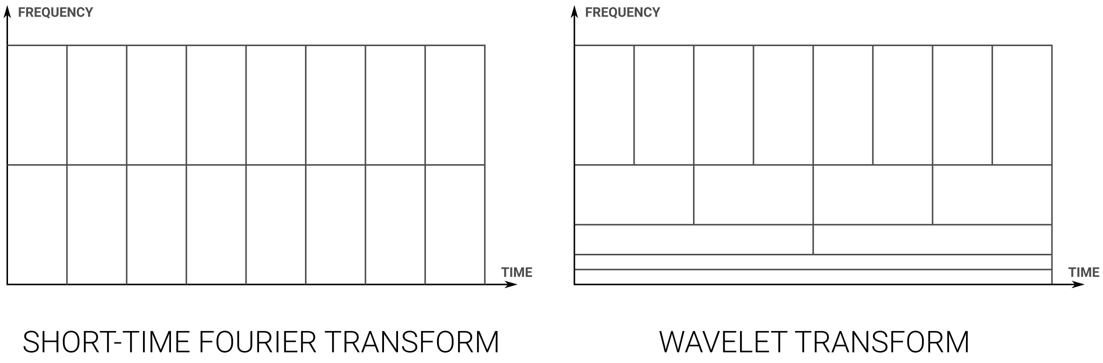

SHORT-TIME FOURIER TRANSFORM

WAVELET TRANSFORM

Figure 2.2: Comparison of short-time Fourier transform with wavelet transform in terms of how they partition the time-frequency domain

a dyadic layout where it allocated higher frequencies more samples, whereas frequency ranges are more refined for lower frequencies. An example is given in Figure 2.2. As it can be seen, wavelet transform actually applies a more reasonable trade-off between time and frequency resolutions, by having more time samples where frequencies change rapidly (high-frequency components), and vice versa. Wavelet transform depends on two functions called the mother wavelet function and the scaling function [37], and different functions can provide different wavelets, each of which might be more appropriate for a certain task than others. At each step, the input signal is passed through a high-pass filter and a low-pass filter, after which both outputs are downsampled by 2. The process is iterated on the low-frequency side until the size of the coefficient is equal to 1. Figure 2.3 depicts the process, and a simple example is described while discussing Haar wavelets.

2.1.3.1 Haar Wavelet

Haar wavelet the simplest form of wavelet transform.

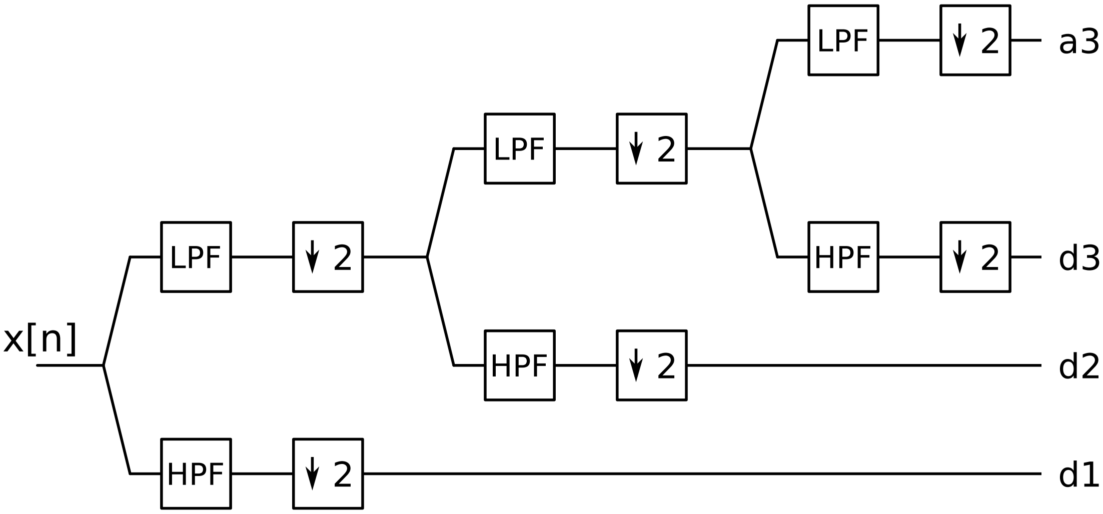

Figure 2.3: Wavelet transform. At each step, detail and approximation coefficients are generated with half the input length. Approximation coefficients are applied the same process until the output length is 1.

The mother wavelet function for Haar transform is defined as:

$$\psi(t) = \begin{cases} 1 & \text{if } 0 \leq t < \frac{1}{2}, \\ -1 & \text{if } \frac{1}{2} \leq t < 1, \\ 0 & \textit{otherwise}. \end{cases}$$

and the scaling function is:

$$\phi(t) = \begin{cases} 1 & \text{if } 0 \leq t < 1, \\ 0 & \textit{otherwise}. \end{cases}$$

An example of the Haar wavelet decomposition on a discrete signal is given in Figure 2.4. In the first step, each pair of elements effectively generate two coefficients, such that $a_1[t] = \frac{1}{2}I[2t] + \frac{1}{2}I[2t+1]$ and $d_1[t] = \frac{1}{2}I[2t] - \frac{1}{2}I[2t+1]$ (for a correct Haar transform each of these equations should have been multiplied with $\sqrt{2}$ for energy preservation but we will omit this detail for simplicity). Effectively, a low pass filter and a high-pass filter with cut-off frequencies $f_c = f_s/4$ are applied onto the input (the frequency responses of which can be seen in Figure 2.5), then the result is downsampled with a factor of two. The a_1 are the 1^{st} level

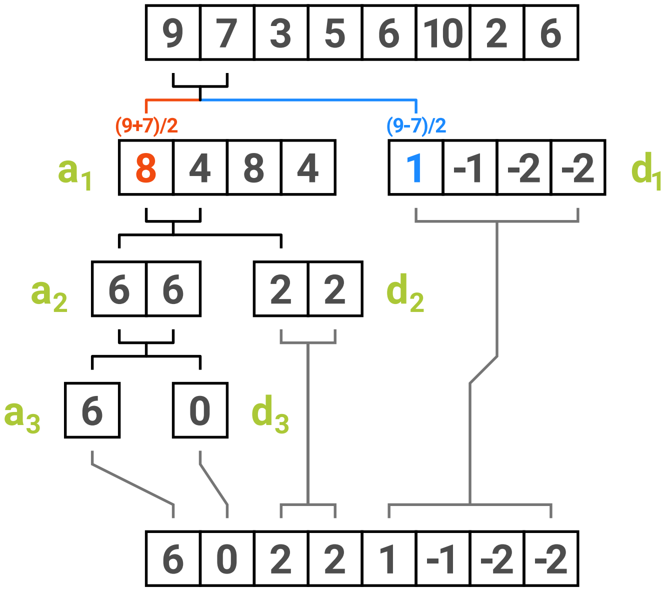

Figure 2.4: An example to the Haar wavelet transform

'approximation' coefficients, whereas d_1 are the 1^{st} level 'detail' coefficients. This process is then iteratively repeated on the approximation coefficients, until the length of both sides is 1. Given that the initial length of data is 2^N for an integer N, the total number of resulting coefficients will have a length of 2^N as well.

Note that at each step we iterate over the approximation coefficients only. The reason is that the approximation coefficients represent the lower frequencies whereas detail coefficients consist of the high-frequency information. It follows that the low frequency components of a given signal tend to change more slowly whereas high-frequency information quickly changes; therefore it makes sense allocating more samples to represent the detail coefficients. This corresponds to a separation of the time-frequency plane in a different way than that of the short-time Fourier transform, as seen in Figure 2.2.

Once the wavelet coefficients are obtained, perfect reconstruction of the samples is possible within the limitations of the given quantization scheme [37]. For Haar wavelets, $I[2k] = a_1[k] + d_1[k]$ and $I[2k+1] = a_1[k] - d_1[k]$. For our example, $I = \{(8+1), (8-1), (4+(-1)), (4-(-1)), (8+(-2)), (8-(-2)), (4+(-2)), (4-(-2))\} = \{9, 7, 3, 5, 6, 10, 2, 6\}$, which is equal to the initial signal.

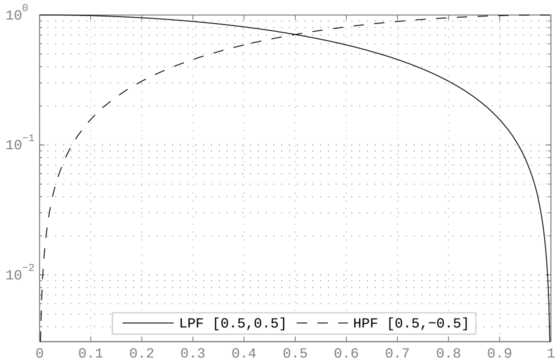

Figure 2.5: Frequency responses of the high-pass and low-pass filters that are used in the Haar wavelet decomposition process. The y-axis is the logarithm of magnitude, the x-axis is the normalized frequency.

Furthermore; if we were to set every d_1 coefficient to zero, the reconstruction would yield $I' = \{8, 8, 4, 4, 8, 8, 4, 4\}$; which is a rather close approximation of the initial signal. Technically speaking, we would have suppressed the high frequency components; and practically filtered the signal. Selecting the detail and approximation coefficients that correspond to the frequency bands we want and setting the others to be zero would effectively give us these frequency bands.

One disadvantage of Haar wavelets is that despite their simplicity, they lack differentiability, since the function is explicitly discrete. Another issue that arises can be seen from Figure 2.5, as the filters that correspond to the transform operation do not very effectively separate the two frequency bands; therefore Haar wavelets cannot achieve a very good resolution in terms of frequency.

2.1.3.2 Daubechies Wavelet

Daubechies wavelets can be considered as a generalization of Haar wavelets, for Haar wavelet is also known as Daubechies-2 wavelet (D2) [38]. To provide a crude perspective, whereas scaling sequence provides a low-pass filter, wavelet sequence acts as a band pass filter. Daubechies presented a family of wavelets with a filter

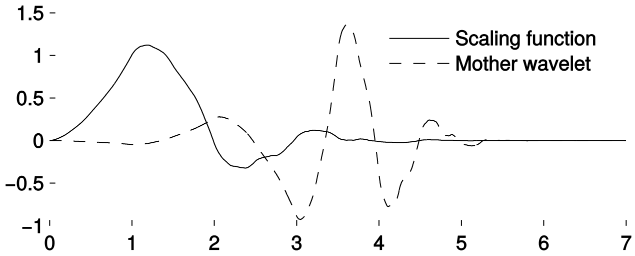

Figure 2.6: An example to the Daubechies-4 wavelet transform

size of $2p$, by solving the equation below using Bezout theorem [39]:

$$H_\phi(e^{iw}) = \sqrt{2}\left(\frac{1+e^{-iw}}{2}\right)^p R(e^{iw})$$

For p=2, the obtained polynomial is:

$$P(\frac{2-z-z^{-1}}{4}) = 2 - \frac{1}{2}z - \frac{1}{2}z^{-1}$$

of which the roots are $2+\sqrt{3}$ and $2-\sqrt{3}$. The discrete-time factorization is then:

$$h_\phi[n] = \frac{\sqrt{2}+\sqrt{6}}{8}\delta[n] + \frac{3\sqrt{2}+\sqrt{6}}{8}\delta[n-1] + \frac{3\sqrt{2}-\sqrt{6}}{8}\delta[n-2] + \frac{\sqrt{2}-\sqrt{6}}{8}\delta[n-3]$$

This gives us the Daubechies-4 wavelet transform, or “D4” in short [39], the scaling and wavelet functions for which are given in Figure 2.6.

Other wavelet families with different derivations exist, however they are beyond our scope, because many papers regarding heart sound segmentation use Haar and D4 wavelets [6, 18, 19, 30]. This makes sense due to a comparison between wavelet families that revealed that D4 is optimal for heart sound analysis [10].

2.1.4 S-Transform

S-Transform is a special variation of STFT such that it allows variable window sizes [40]. In S-Transform, the window function $w(t)$ is selected as

$$w(t) = \frac{|f|}{\sqrt{2\pi}} e^{-t^2 f^2/2}$$

therefore S-transform is defined as

$$S(t, f) = \int_{-\infty}^{\infty} x(k) \frac{|f|}{\sqrt{2\pi}} e^{-(t-k)^2 f^2/2} e^{-i2\pi f k} dk$$

Although S-transform can provide a good resolution, its computational complexity is as high as $\mathcal{O}(N^3)$ [41]. An FFT-based implementation has a computational complexity of $\mathcal{O}(N^2 log_2(N))$ [42], which requires that the acquisition of the entire signal is completed. It is possible to reduce the computational complexity of S-transform further down to $\mathcal{O}(N log_2(N))$ using approximations [41]; of which the implementation might lead to madness [43].

2.1.5 Constant-Q Transform

Constant-Q transform maps the linear frequency domain of a Fast Fourier Transform onto a logarithmic frequency domain [44], such that the k^{th} frequency component is at $f_k = 2^{k/24} f_{min}$. Originally being designed for the geometric positioning of musical notes, Constant-Q transform separates every octave into 24 intervals; hence the $k/24$. f_{min} is the minimum sampled frequency for which information is desired. The name Constant-Q comes from the fact that the window on which discrete Fourier transform is performed is selected to have the length of Q cycles, where Q is a constant. In regular DFT where the k^{th} frequency component is at $k\delta f$, the number of cycles becomes variable, *i.e.* dependent to k.

Here, Q is named the quality factor [45]. The equation becomes the one below:

$$X[k] = \frac{1}{N[k]} \sum_{n=0}^{N[k]-1} W[k,n]x[n]e^{-i2\pi Qn/N[k]}$$

where

$$N[k] = N_{max}2^{-k/24}$$

and

$$W[k,n] = \alpha + (1-\alpha)cos(2\pi n/N[k]).$$

which is a Hamming window adapted to the exponential frequency [45].

2.2 Maximal Marginal Relevance

Maximal Marginal Relevance (often abbreviated as MMR) is a method first proposed by Carbonell and Goldstein for text retrieval and summarization [33]. In a context where sorting a retrieved document set S with respect to their relevance with a given query Q produces redundant or repetitive results, diversity becomes a desirable property. A result set is said to be diverse if the retrieved documents are dissimilar to each other. Diversifying the result set helps represent a large variety of topics in the top results, while avoiding highly similar (or even duplicate) results.

Assume that for a given document collection C; the information retrieval system $R = IR(C, Q, \theta)$ retrieves a ranked list of documents R that have a similarity with the query Q above a given relevance threshold θ. then the maximal marginal relevance is calculated as follows:

$$MMR = \arg \max_{D_i \in R \setminus S} \left[\lambda Sim_1(D_i, Q) - (1-\lambda) \max_{D_j \in S} Sim_2(D_i, D_j) \right]$$

Here, S is the subset of R that is to be returned. Initially $S^{(0)} = \emptyset$. At each k^{th} iteration, $S^{(k)} = S^{(k-1)} \cup MMR$. In other words, S contains the elements that are already picked, and the next element is chosen from the difference set

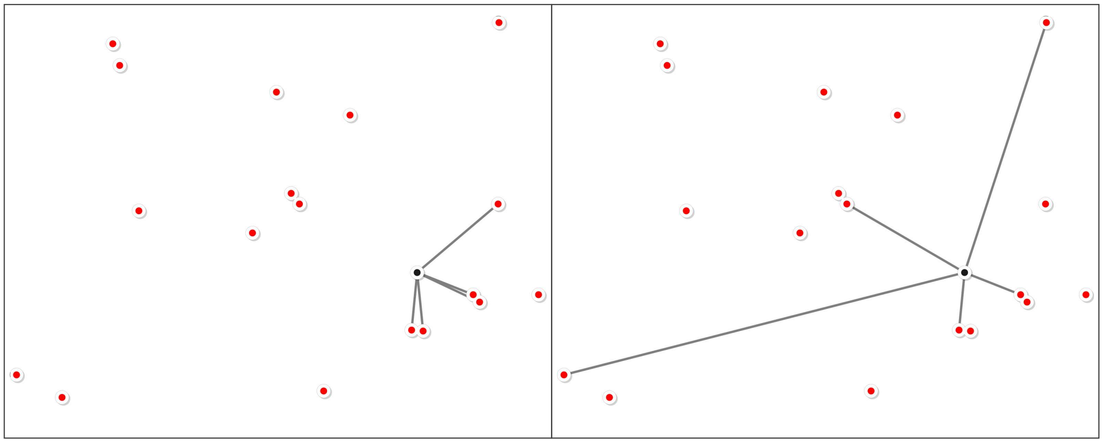

Figure 2.7: Top-5 results without MMR (left) and with MMR (right, $\lambda = 0.5$). Black point represents the query.

$R \backslash S$ such that it both maximizes the similarity to the query, and minimizes the maximum similarity to any element in S. The parameter $\lambda \in [0, 1]$ tunes the relative importance of these two factors against each other.

Since initially S is an empty set; initially $R \backslash S = R$ and $\max_{D_j \in S} Sim_2(D_i, D_j)$ is 0. Therefore $D_1 = \arg\max_{D_i \in R} Sim_1(D_i, Q)$, meaning, the first picked element D_1 will be the most similar one to the query Q. After this, next element will be both similar to Q and dissimilar to D_1 (more formally; $\arg\max_{D_i \in R \backslash \{D_1\}} [\lambda Sim_1(D_i, Q) - (1 - \lambda) Sim_2(D_i, D_1)]$), and so on.

Figure 2.7 depicts an example of the MMR algorithm. Here, $Sim_1(x, y) = Sim_2(x, y) = \frac{1}{||x-y||^2}$, that is, geometric inverse of the squared Euclidean distance. It can be seen in the second subfigure that similarity is traded off with diversity, such that data points that are redundantly similar to one another are not picked.

We will use this equation to pick large but diverse samples in the time series of the heart sound signal, representing separate peaks.

Chapter 3

Related Work

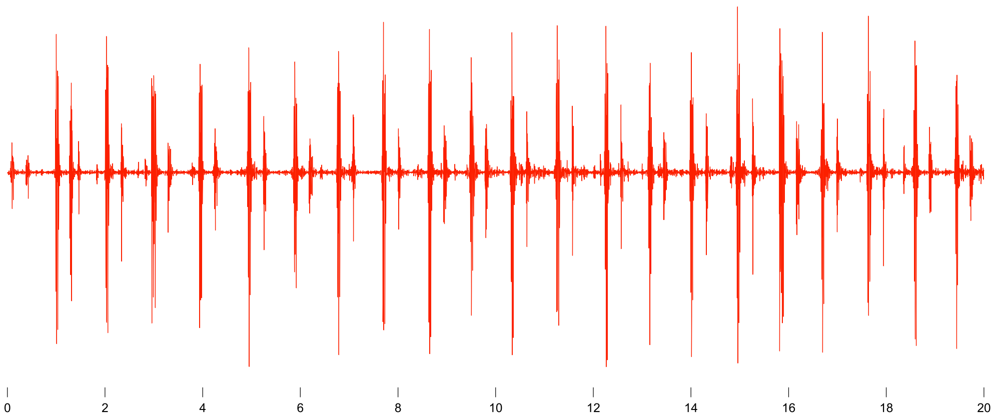

Figure 3.1: Normal heart sound recording, depicting the heart sounds S_1 and S_2 [46]

The detection and separation of cardiac cycles with the intent of recognizing heartbeats is named "heart sound segmentation". Since heart murmurs with differently distributed energies within the cardiac cycle may reflect different clinical conditions, a good segmentation algorithm is essential for detecting the temporal locations of such events with respect to the regular cardiac cycle events.

The mammal heart consists of four chambers, symmetrically separated into two sides. The contraction of these chambers sequentially, combined with four unidirectional valves, effectively pumps blood in one direction. Two audible sounds are generated during these contractions, namely the *first heart sound* (S_1) and the *second heart sound* (S_2), also occasionally referred to as the 'lub' and the 'dub' (or 'dup') [10]. The interval from one S_1 to the next is named a *cardiac cycle*. Therefore, each cardiac cycle also contains an S_2 peak. This S_2 peak separates the cardiac cycle into two sub-intervals: The interval between S_1 and the following S_2 is called a *systolic period*, whereas the interval between an S_2 and the next S_1 is called a *diastolic period* [6]. In total, a cardiac cycle consists of an S_1 peak, a systolic period, an S_2 peak, and a diastolic period in the given order. Typically, the diastolic period of a given cardiac cycle has a longer duration than its systolic period.

A heart sound recording may include other sounds, some of which are inaudible without amplification (for example, S_3 and S_4). However, S_1 and S_2 are the only heart sounds that are commonly expressed in any phonocardiogram, therefore these two sounds are used by every segmentation algorithm unanimously.

There are various challenges that makes the segmentation task non-trivial. First of all, heart sound recordings are very noisy, and the assumptions made on a certain dataset do not hold for another. The source of noise is not only electronic, but also mechanical; including but not limited to the reverberations of heart sounds from internal tissues, sharp peaks originating from sudden movements of the stethoscope, abnormalities in the heart and so on [32]. Attempts at removing these noises by isolating S_1 and S_2 sounds in their frequency bands do not work well, because not only these noises may occur at any frequency band, but also S_1 and S_2 have different frequencies at every patient and even between cycles [10]. Although attempts have been made to eliminate lung sounds from these recordings [32], a reliable method for the removal of the noises in phonocardiograms, clearly expressing S_1 and S_2 sounds, remains to be discovered. Therefore, segmentation algorithms try to employ approaches specific to the characteristics of the heart sound signal, depending heavily on assumptions obtained from medical observations [6, 15, 17, 23–26, 29–32]. Even though there have been attempts at designing heart sound classification techniques that do not depend on segmentation [22], these are reported to show a more robust performance on segmented data [11]. Therefore, heart sound segmentation remains to be a 'bottleneck' for the performance of many algorithms proposed for heart disease detection and classification.

Another challenge in this line of research is that most of the methods in the literature have been tested on the datasets that were preprocessed and curated exclusively and are kept private. This means that there is no guarantee that a particular method that is tested on a given dataset would provide a similar performance on another dataset. A proper unification and comparison of these methods on a common reliable dataset is missing.

There has been extensive work regarding the cardiac cycle segmentation problem in the last two decades. Two major subsets of these approaches are ECG based segmentation and PCG segmentation. While ECG segmentation algorithms use the electrocardiogram signal to segment the phonocardiogram, PCG segmentation algorithms only receive the heart sound waveform as input.

3.1 ECG Segmentation

There are various heart sound segmentation algorithms using the electrocardiogram signal as reference. The advantage of this approach is that ECG signal is not affected by heart murmurs, which are not electrical events; which makes it desirable for industrial applications. Dominant peaks in PCG envelope might not be strongly correlated with cardiac activities in the presence of strong abnormal sounds [28]. Therefore the performance of a PCG segmentation algorithm can be rather sensitive to abnormalities when compared to an ECG-aided segmentation algorithm.

Given the PCG and ECG recordings, an ECG segmentation starts by attempting at segmenting the ECG signal first [47]. A QRS detection method such as Tompkins algorithm [12] is applied onto the ECG signal to locate the R waves. It is observed that R waves are temporally correlated with S_1 sounds; therefore S_1 sounds in the PCG signal must be in the vicinity of R waves in the ECG signal [28]. One approach is to call the interval between two R waves a cardiac cycle, and try to detect S_1 and S_2 sounds within each cardiac cycle [21]. Another is called "ECG gating", and involves searching S_1 in the predefined neighborhood

of the R waves, then looking for S_2 peaks in between [16,17].
There are several advantages of such segmentation algorithms. First of all, the presence of murmurs does not affect the ECG waveform, thus the performance of the algorithm [10]. Segmentation of ECG signals is relatively easier and rather well-studied compared to PCG signals. Finally, reported accuracies of ECG segmentation algorithms are typically higher than PCG segmentation algorithms.
However, these algorithms require an ECG signal to be recorded along with PCG in the first place. Considering that the design objective we have set was minimizing hardware requirements to reduce cost and increase availability, this approach seems misplaced. Also, precise temporal alignment of PCG and ECG signals is necessary for ECG-aided segmentation algorithms to operate, since they require that the segmentation obtained in one can be mapped onto the other; which requires a synchronous operation of two independent systems, with good temporal precision non-trivial to achieve. Finally, even though ECG signal is segmented properly, S_1 and S_2 sounds are still looked up on the PCG signal. Especially the location of S_2 can be affected as significantly in the presence of strong murmurs. Therefore we turn our gaze towards PCG segmentation algorithms permanently from this point on.

3.2 PCG Segmentation

PCG segmentation algorithms do not use any secondary external signals such as ECG waveforms to achieve segmentation. Rather, segmentation itself is achieved directly on the PCG waveform. Since heart abnormalities make themselves apparent on the heart sound, they can affect the performance of the segmentation algorithm. However, this is the only desirable approach to the problem in terms of cost, since it does not require the installation, synchronization and acquisition of any external module such as an electrocardiogram. Since heart sound signals are highly organic signals, it is very difficult to find a constant factor in them. Often, the temporal lengths of every systolic and diastolic period deviate. Even though S_1 and S_2 are assumed to be highly audible, their amplitudes might change significantly, to the point of disappearance in the presence of certain abnormalities. Finally, S_1 and S_2 peaks do not seem to have fixed frequencies, but rather present themselves within different frequency bands in two separate cardiac cycles. These limitations of the heart sound signal led researchers to develop a rather unique approach to heart sound segmentation. The general approach to PCG segmentation can be found in [6, 23, 25, 29, 31, 32].

One of the earliest solutions that was dependent on only the PCG signal was proposed in [27]. The idea was to threshold the absolute value envelogram of the signal after it was passed through a band-pass filter. Although this approach was defined to be easy to implement on an analog circuit, Liang et al. extended and refined the idea significantly in [29]. The suggested methodology has several steps, and inspired many other papers in the field in terms of the approach to be taken towards the solution of the problem. In order to discuss all these papers in a unified frame, we describe the methodology with a slightly enhanced separation of steps as below:

STEP 0: Preprocessing

STEP 1: Time-frequency transformation

STEP 2: Transformation to a non-negative domain

STEP 3: Envelope detection

STEP 4: Picking up peaks

STEP 5: Rejection and merging of extra peaks

A vast majority of heart sound segmentation algorithms (reminding the reader that ECG segmentation algorithms are out of scope at this point) follow this general pattern with variations in each step [6, 11, 13, 15–19, 23, 25, 27–32]. Other approaches include Mel-cepstrum analysis [22], SAX-based multiresolution motif discovery [48] and matching pursuit method [10].

11025	→	2205 Hz	[6, 29, 31]
8000	→	2000 Hz	[18]
8000	→	4000 Hz	[23]
44100	→	4410 Hz	[13]
44100	→	4096 Hz	[16]

Table 3.1: Decimation schemes of various PCG segmentation algorithms

3.2.1 Step 0: Preprocessing

The preprocessing step involves the re-sampling and normalization of the original recording.

Liang et al. worked with heart sound recordings with a sampling frequency of $f_s = 11025$ Hz. The frequency of the recordings was decimated to $f_s = 2205$ Hz, and then the signals were normalized. Before the downsampling step, the signal is passed through a Chebyshev Type-I low pass filter with a cut-off frequency at 882 Hz. Downsampling is required for avoiding redundant sampling of a signal where only the $50 - 700$ Hz range contains clinical information [23].

The normalization of the signal is achieved as below:

$$x_{norm}(t) = \frac{x(t) - \mu}{\sigma}$$

where μ is the mean of $x(t)$, and σ is the standard deviation[19]. Gupta et al. later report that the performance of the algorithm is negatively affected by this normalization scheme [23], and used the formula

$$x_{norm}(t) = \frac{x(t)}{\max\limits_{t \,\in\, \mathbb{R}} |x(t)|}$$

which limits x_{norm} within the $[-1, 1]$ range.

Generally, the original recordings are re-sampled to a sampling frequency either around 4000 Hz, or 2000 Hz. Table 3.1 lists the decimation schemes employed by several papers.

In our study, we use the Pascal heart sound classification challenge dataset [1] which has a sampling frequency of 44100 Hz. We decimate these signals to 4410 Hz first. Initially we were to receive annotated heart sounds recorded by the 3M$^{\text{TM}}$ Littmann$^{®}$ electronic stethoscope, for which $f_s = 4000$ Hz [18]. The signals were to be normalized and used as is.

3.2.2 Step 1: Time-Frequency Transformation

Often, the received heart sound recording contains substantial amount of noise and irrelevant information. Therefore many authors employ a time-frequency transform by which certain frequency bands are considered. Initial papers such as [29] did not have any frequency band selection/suppression step. Vepa [11] and Delgado-Trejos et al. [13] used the Short-Time Fourier Transform to suppress irrelevant frequency bands. Strunic et al. [15] obtained the spectrogram of the signal and used the 45 Hz band for segmentation, upon the observation that both S_1 and S_2 peaks present themselves at that frequency band. Livanos et al. [25] compared S-transform with Morlet wavelet and STFT. Mondal et al. [32] proposed using Hilbert transform and Heron's formula in order to eliminate lung sounds mainly.

Upon the observation that D4, Meyer and Morlet wavelets are optimal for heart sound analysis [10], wavelet transform has been preferred by many works [6, 17–19, 30]. Since S_1 and S_2 sounds may express themselves at variable frequencies that may not be contained in a single wavelet band, several wavelet bands are considered at once in parallel [6, 30].

In our work, we will be considering four wavelet bands as d7, d6, d5 and a5; corresponding to the frequency bands $\left[\frac{f_s}{128}, \frac{f_s}{64}\right]$, $\left[\frac{f_s}{64}, \frac{f_s}{32}\right]$, $\left[\frac{f_s}{32}, \frac{f_s}{16}\right]$, $\left[0, \frac{f_s}{32}\right]$ respectively. For $f_s = 4096$ Hz, these frequency bands correspond to 32-64 Hz, 64-128 Hz, 128-256 Hz and 0-128 Hz respectively. Our application converts any signal into a sampling frequency of either 4000 Hz or 4410 Hz, therefore the frequency ranges will have very similar boundaries.

3.2.3 Step 2: Transformation to a Non-Negative Domain

Normal heart sound activities such as S_1 and S_2 behave similar to amplitude modulated signals [23]. Extracting the envelope of the signal is therefore essential for further analysis, which first requires the signal to be 'rectified' into the non-negative y-axis (Step 2). Liang et al. [29] tried four different equations to map the original signal to the non-negative domain, as shown in Figure 3.2:

$$\begin{aligned} \text{Absolute value:} \quad & E = |x| \\ \text{Energy (square):} \quad & E = x^2 \\ \text{Shannon entropy:} \quad & E = -|x| \log |x| \\ \text{Shannon energy:} \quad & E = -x^2 \log x^2 \end{aligned}$$

Shannon energy emphasizes the medium energy signal more efficiently, and attenuates low and high intensity signals, which helps suppress noise; therefore used by most of the future applications [17, 18, 29, 30, 49]. Although Shannon entropy shares this property, it further accentuates the low intensity noise [49].

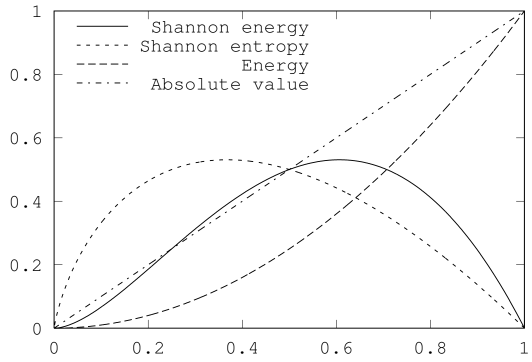

Figure 3.2: Non-negative transforms

3.2.4 Step 3: Envelope Detection

After the time-frequency transform and rectification (which, at this point, we can call *energy calculation*), the temporal locations at which the amplitude exceeds a certain threshold should be detected. However, the signal is still not smooth enough for such an operation; especially noise around the threshold may cause redundant peaks caused by the fluctuations.

In this step, the envelope of the signal is calculated in order to get rid of noise and smooth the peaks. Liang et al. [29] used the envelogram approach, where the rectified signal is averaged over tumbling time windows of 20 ms length, with 10 ms overlap. The length of 20 ms windows correspond to $N = \lfloor t \cdot f_s \rceil = \lfloor 0.02 \text{ s} \cdot 2205 \text{ Hz} \rceil = \lfloor 44.1 \rceil = 44$ samples in their case. Note that in the original paper Step 2 and Step 3 are described as one step as below:

$$E_s = -\frac{1}{N} \sum_{i=1}^{N} x_{norm}^2(i) \cdot \log x_{norm}^2(i)$$

Here, x_{norm} is the normalized and decimated signal obtained in Step 0. This approach has been also employed by other papers [18, 32].

Another approach is to apply a homomorphic filter onto the signal [20, 23]. Since the heart sound recording have similar characteristics to that of an amplitude-modulated signal; it can be considered as the multiplication of a high-frequency carrier signal $HF(t)$ and a low-frequency message $LF(t)$ (which we want to obtain) [23]. Then the original signal is $f(t) = HF(t) \cdot LF(t)$. Taking the logarithm of both sides gives us

$$log(f(t)) = log(HF(t)) + log(LF(t))$$

Assume that we have a low pass filter LPF that can perfectly suppress $HF(t)$ and leave $LF(t)$ as is. Then the homomorphic filter is defined as

$$\begin{aligned} e^{LPF\{log(f(t))\}} &= e^{LPF\{log(HF(t))+log(LF(t))\}} \\ &= e^{log(LPF\{HF(t)\})+log(LPF\{LF(t)\})} \\ &= e^{log(LF(t))} \\ &= LF(t). \end{aligned}$$

Clearly, the method assumes that $log(f(t))$ is defined; that is, $f(t) > 0$ for all t.

Our tests revealed that both methods return very similar envelopes, therefore we proceeded with the envelogram method.

3.2.5 Step 4: Picking Up Peaks

Once the envelope is obtained, a threshold is applied onto the signal in order to obtain peak candidates. Any interval that exceeds this threshold is considered a peak candidate. The highest point in the interval becomes the center of the peak, and the width of the interval is considered the peak width.

While the threshold criterion in [29] is not given, the figures in that paper show slightly different thresholds between 0.75 and 0.8. One method to select a threshold automatically is using the mean of the envelope. Gupta et al. used 35% of the maximum peak as the threshold value instead [23]. Hedayioglu selected $thr = 0.5\left(\max_{t\in\mathbb{R}} E_s(t) + \min_{t\in\mathbb{R}} E_s(t)\right)$ as the threshold [6].

3.2.6 Step 5: Rejection and Merging of Extra Peaks

Not all peak candidates might be actually meaningful, nor can we assume that we have picked every relevant peak. In order to merge the extraneous peaks that might have been obtained in the thresholding step, Liang et al. proposed a set of rules as described below [29]:

1. The intervals between adjacent peaks are calculated.
2. *Low-level time limit and high-level time limit are calculated* using intervals.
3. If the interval is less than the low-level time limit, one of the peaks is extra (*i.e.* redundant).

- 50 ms is the largest splitted normal sound interval observed. Therefore if two peaks appear within 50 ms of each other, this is assumed to be due to a split heart sound. If the energy of the first peak is *not too small* compared to that of the second one, the first peak is selected.
- Otherwise, the second one is selected.

4. If the interval is greater than the high-level time limit, it is concluded that a peak was too weak to be detected. Lower the threshold *by a certain amount*, and repeat.

There are three uncertainties in the set of rules above, shown in italic. First of all, low-level and high-level time limits are not well defined. We assume that these values are obtained as below:

$$\begin{aligned} \text{Low-level time limit} &= \mu - c_1 \cdot \sigma \\ \text{High-level time limit} &= \mu + c_2 \cdot \sigma \end{aligned}$$

where μ is the mean of intervals, and σ is the standard deviation such that

$$\mu = \frac{1}{N-1} \sum_{i=1}^{N-1} p_{i+1} - p_i, \qquad \sigma^2 = \frac{1}{N-1} \sum_{i=1}^{N-1} [(p_{i+1} - p_i) - \mu]^2$$

where $P = \{p_1, p_2, \cdots, p_N\}$ are the temporal locations of the peaks such that $p_i < p_j$ **iff** $i < j$ (*i.e.* peaks are sorted). Hedayioglu also makes the same assumption [6].

Another uncertainty is the "not too small" expression in the elimination process.

Once all peaks are within a reliable margin, the algorithm decides which peaks are S_1 and which are S_2. The approach is to select the widest interval and classify it as diastolic, then alternate towards both directions. The idea is that diastolic periods are always longer than systolic periods, therefore the longest period should be diastolic. Any peaks between a systolic and a diastolic period is an S_1, and vice versa.

Gupta et al. implemented a similar algorithm to that of Liang et al. in [23]:

1. Peaks closer than 80 ms are combined into a single peak.
2. Mean peak width is calculated.
3. Any peaks with width less than half the mean peak are considered to be noise and rejected.
4. Peaks wider than 120 ms are limited to 120 ms.

Haghighi-Mood and Torry [28] proposed an intermediary step in which a morphological transform is applied in order to get rid of the peaks that might have been generated by the existence of murmurs. Their assumption is that the S_1 and S_2 peaks are sharp whereas murmurs are more likely to generate wider peaks. Their idea is to suppress each peak according to its width. If $P = \{p_1, p_2, \cdots, p_k\}$ is the sorted set of all peaks above a threshold of -25 dB; then

$$E_{sm}(k) = \begin{cases} E_s(k) - 0.5\left[E_s(p_i - \ell) + E_s(p_i + \ell)\right] & \text{for } p_i - \ell \leq k \leq p_i + \ell \\ 0 & otherwise \end{cases}$$

After this, S_1 and S_2 sounds are determined using K-means clustering. Hedayioglu further simplified this final step using the basic assumption that a diastolic period is always longer than the systolic period; therefore the median of all intervals should easily separate the interval set into systolic and diastolic intervals given that the number of S_1 peaks is equal to the number of S_2 peaks that are detected [6]. After labeling each interval; any peak that comes before a systolic period is S_1, and vice versa.

3.2.7 Results

Liang et al. defined a correctness ratio as the fraction of correctly determined peaks, and reported a correctness ratio of 93%, having detected 479 peaks out of 515 correctly. However, this measure needs to be extended for the cases where a peak is missed, an extra peak is included, a peak is detected properly but labeled with the wrong name, or a peak is detected but shifted by a certain amount.

Hedayioglu implemented Liang et al.'s algorithm and reported an accuracy of 49.32% on another dataset [6]. Hedayioglu's algorithm, which includes the parallel analysis of four wavelet bands and a better S_1 - S_2 classification approach has a reported accuracy of 61.85% on this dataset. The difference between 93% and 49% is presumably due to different interpretations of which peaks to count as correctly identified, or the datasets that were used.

As there has been no benchmark in the literature that includes a common evaluation measure and a common data set, the current methods results are virtually incomparable. Our first aim is to implement all these methods with the intent of testing them all using a common dataset and well-defined evaluation metrics.

Chapter 4

Data Acquisition and Annotation

The privacy regulations imposed upon medical data makes public heart sound recording data sets scarce. It is typical that the authors curate their own datasets, as well as annotate these recordings. However annotation of heart sounds requires marking the samples at which each peak occurs; and this should be done by hand. Therefore properly annotating a dataset requires extensive work, and a knowledge of signal processing environments such as MATLAB, with which a medical doctor may not necessarily be familiar. Even then the task is cumbersome; and requires attention. For example, the annotations provided in the Pascal dataset include two files where the sample numbers have been incorrectly noted down [1]. As long as the user cannot see the actual position of the annotated samples, the datasets provide little or no intuition upon inspection. Therefore the need arose to develop a simplistic tool for heart sound visualization, playback and annotation with an easy-to-use, drag-and-drop interface.

Although we ended up using a subset of the Pascal heart sound classification challenge dataset as our test set [1]; initially we planned to curate our own dataset. Collection of the heart sound recordings were to be conducted using a 3M$^{\text{TM}}$ Littmann$^{\circledR}$ electronic stethoscope, which provides .wav files with a sampling frequency of 4000 Hz. We developed an application named UpBeat, with an intuitive graphical user interface to simplify the annotation process significantly.

UpBeat is capable of providing automatic segmentation, which then can be refined manually.

4.1 UpBeat: Heart Sound Segmentation and Annotation Tool

Annotated data for cardiac cycles are essential for developing heart sound models and medical decision support tools. Such collections require significant efforts to generate and are not made publicly available due to several concerns including the privacy of participants. We are aware of only one public data set [1]. Larger and more variant datasets are required for better modeling and avoiding overfitting; therefore an easy-to-use, cross-platform cardiac cycle annotation tool is essential.

There have been few attempts in developing a general-purpose application [15,47], which are mostly dependent on the MATLAB environment instead of a standalone application. We have developed the first open-source, extensible, cross-platform tool in the literature that enables generation of ground truth data for cardiac cycle annotation and segmentation algorithms. The tool provides a benchmark platform for heart sound segmentation, feature extraction for heart disease detection and classification, involves an automatic segmentation algorithm, auditory playback and visual feedback for heart sound training. UpBeat is useful for constructing a medical ground truth for heart sound segmentation, evaluating annotation results, and allows time-domain averaging-based basic feature extraction which is resilient to recordings from different locations with different heart rates. We also introduce the .sgm file format as a general and extensible representation of cardiac segmentation and annotation. Since the algorithms in this thesis are implemented as a Java library, which UpBeat is designed to use, UpBeat can very trivially employ any other automatic segmentation algorithm. We acknowledge that there is still room for improvement in the methods we incorporated, and isolate the segmentation library from the interface.

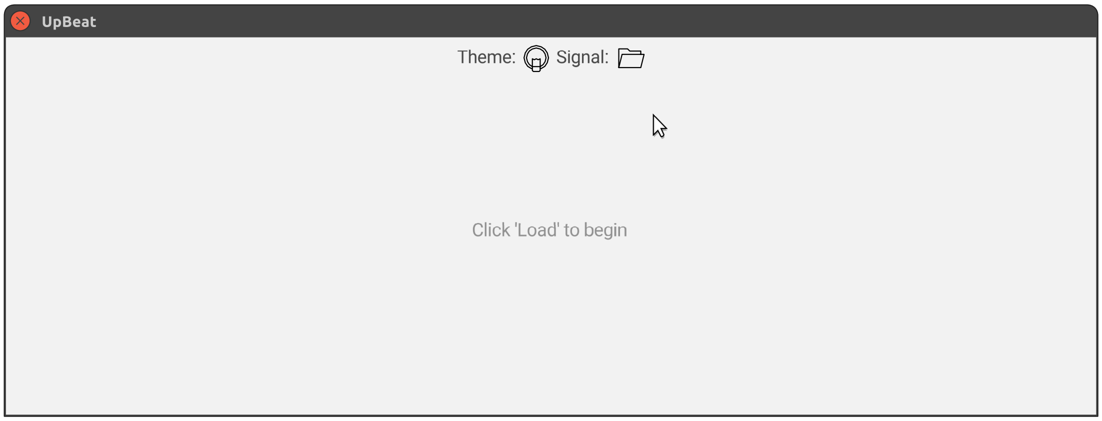

Click 'Load' to begin

Figure 4.1: Initial screen of UpBeat. In order to use the software, one should click on the folder icon and select the .wav file to annotate. Note that the screenshots are also vector drawings, since UpBeat allows for exporting vector screenshots.

Having visual and auditory feedback is crucial for manual annotation of heart sound data. In the absence of such information, correct annotation becomes very cumbersome and requires extreme attention. The peaks in the Pascal dataset are hand-curated and their sample indices are stored in .csv files. We have detected that typos are present in at least two files. Instead of specifying the locations of peaks in terms of seconds or sample indices one by one meticulously in a tabular fashion, we have developed a graphical user interface by which users can visually and aurally perceive and annotate the signal. We have implemented the application in Java using OpenGL bindings that are provided by the JOGAMP library. Using OpenGL allows us to achieve a very fast, flexible and cross-platform interface. The application can be controlled using solely a three-button mouse; or alternatively, only the left mouse button along with a keyboard.

Figure 4.1 shows the initial screen of the program. The only component initially visible is the menu bar. Although the main screen contains more options, two buttons are displayed in the initial screen. The first "bulb" icon is the theme selection icon. Using this, the user can toggle between dark and light themes. The "folder" icon under the "Signal" category lets users to load the .wav file to be annotated into the program. Once a .wav file is selected, the waveform is read and loaded from the file, the automatic segmentation algorithm is executed, and the interface changes to what is seen in Figure 4.2.

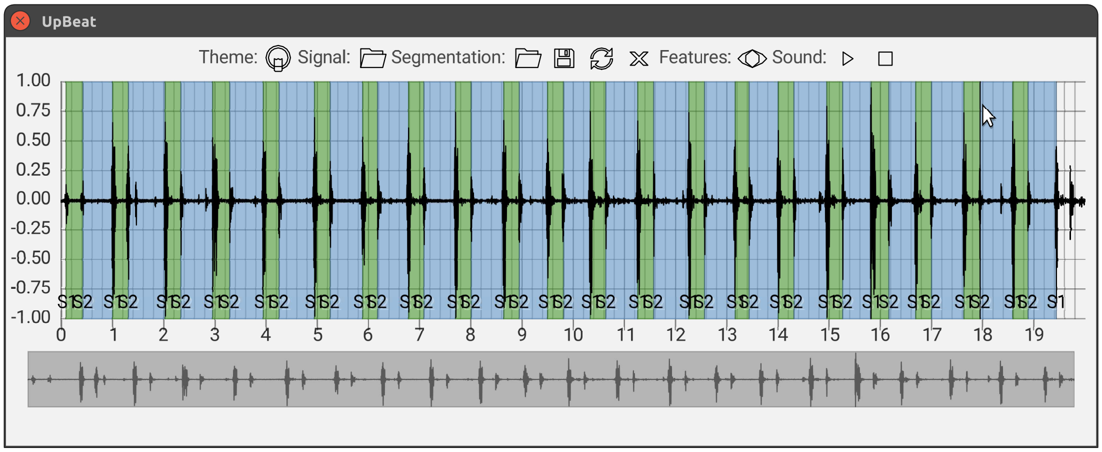

Figure 4.2: Main screen of UpBeat.

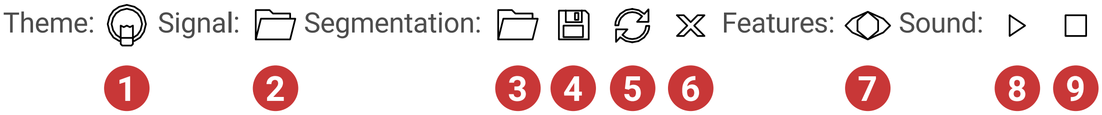

Figure 4.3: Buttons in the main menu, enumerated respectively.

Figure 4.2 is the main click-and-drag interface on which the users are to annotate the waveform. Note that the menu has been extended to include the following categories and buttons, as seen in Figure 4.3:

Theme controls the color themes of the program

1. Toggles between the light and dark themes.

Signal has controls regarding the signal file selection

2. Opens a file dialog to choose the .wav file to be annotated.

Segmentation has controls regarding the annotation process

3. Opens a file dialog to import a previously saved .sgm segmentation file.
4. Opens a file dialog to export the current segmentation into an .sgm file.
5. Overwrites the current segmentation with the automatic segmentation results.

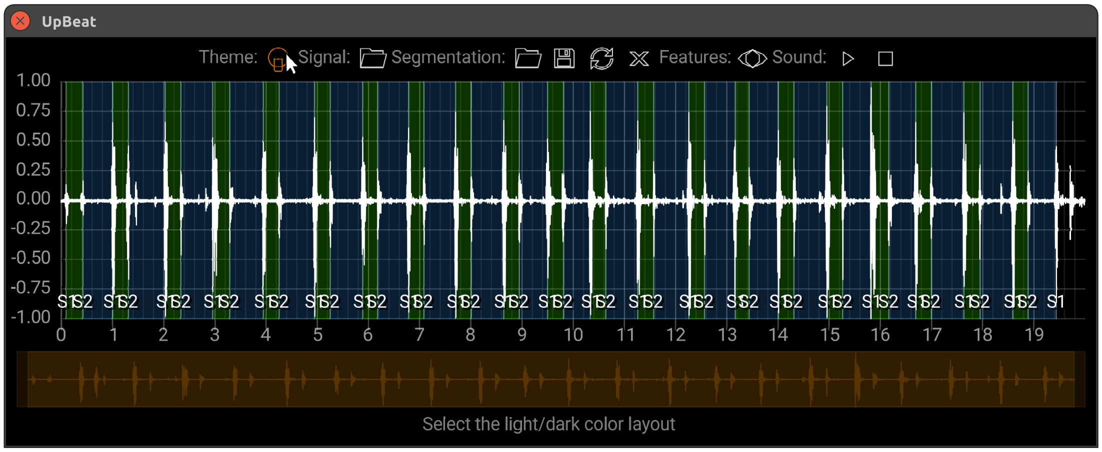

Figure 4.4: Dark theme.

6. Clears the segmentation for the user to start over.

Features has controls regarding feature selection

7. Shows/hides the feature display panel on the right.

Sound has controls regarding audio playback

8. Plays/pauses the heart sound recording
9. Stops the playback

Figure 4.4 shows the dark theme, which can be toggled from the first button in the menu. At the very bottom of the window, hint texts regarding the menu buttons that are hovered by the pointer are shown in the toolbar. Above that is the *zoom bar*. The zoom bar allows the user to magnify a certain time interval on the signal. The zoom bar shows the entire signal, on top of which a box indicates the zoomed region. One can magnify a region of the signal by dragging the handles of the zoom bar to cover that particular area. As the zoom bar is modified, the large waveform in the middle of the screen will be updated to show that particular region, as depicted in Figure 4.5.

Now that the signal in the middle is magnified, we can see the signal and the peaks in more detail. The region shows a normalized version of the signal, where the x-axis is marked to indicate seconds. Note that the signal is automatically

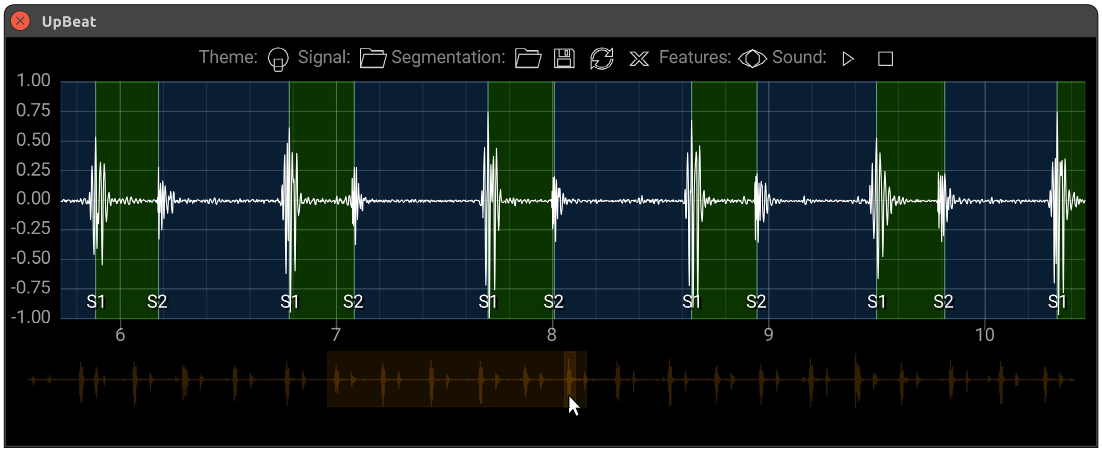

Figure 4.5: Zoom bar example. Notice how the waveform on the zoom bar shows the entire signal, whereas the waveform rendered above is only the yellow section of the zoom bar.

segmented into sections and colored using blue and green. A green region depicts a systolic interval; that is, between an S_1 and the next S_2. A blue region indicates a diastolic interval, which is between an S_2 and the following S_1. An S_2 - S_2 interval is colored in red; whereas an S_1 - S_1 interval is not colored. Each of the peaks is indicated with a vertical white line, and S_1/S_2 texts under them. Editing peaks can be achieved with a 3-button mouse. Left-click adds an S_1 peak (Shift + left-click adds an S_2). Middle click converts an S_1 to S_2 (and vice versa). Right click removes a peak. Existing peaks can also be dragged around. Alternatively, Alt key + left-click serves as the middle click, in the absence of a middle mouse button; and Ctrl + left-click simulates the right-click.

If the automatic segmentation algorithm works with few errors, as it generally does; then a few minor corrections might be enough to complete the annotation process. Otherwise, the cross sign on the menu bar can help reset the segmentation and start over (Figure 4.6).

The user might need to actually listen to the sound to properly annotate the signal. After all, physicians are trained to auscultate and diagnose by ear. The sound category in the menu allows the user to listen to the signal, and meanwhile track the audio position visually. As shown in Figure 4.7, only the magnified region is played in order to avoid confusion.

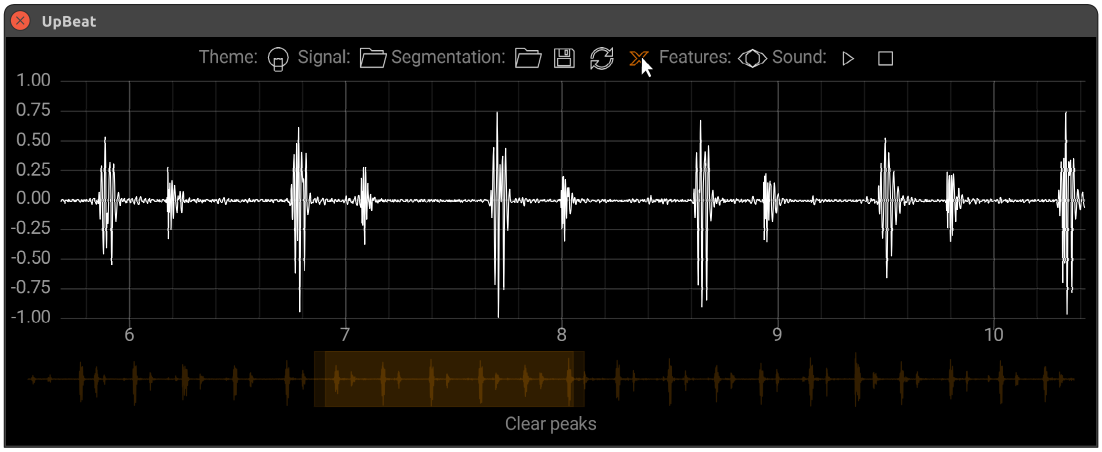

Figure 4.6: Using the clear button, the user can delete the segmentation so far and start over.

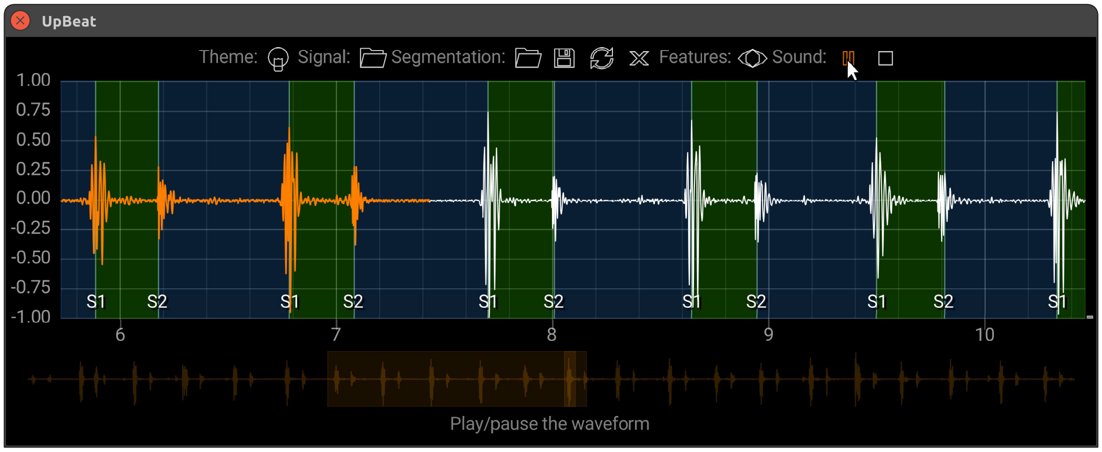

Figure 4.7: The play button allows the user to listen to the heart sound recording, and actually *auscultate*. The progress of the sound is depicted in the middle with the yellow color, so that the physician can know the position of the audio.

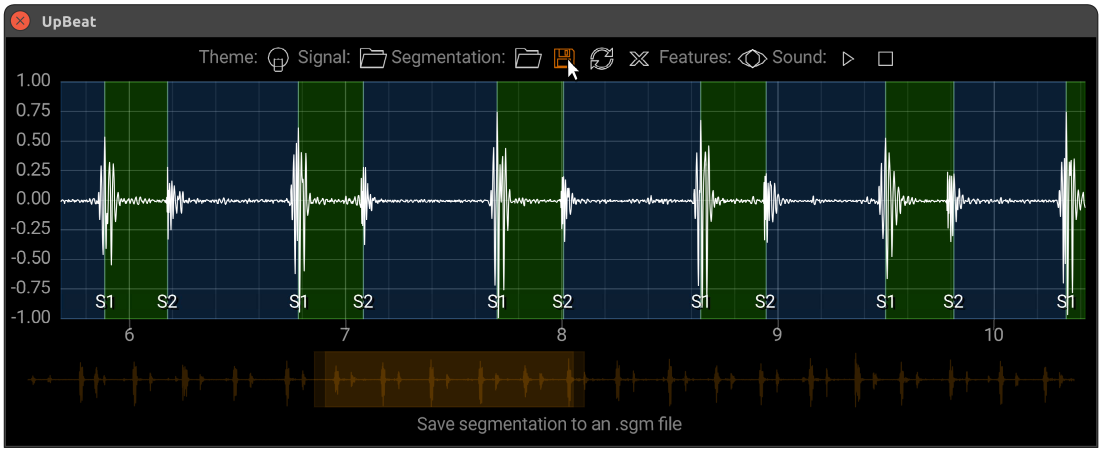

Figure 4.8: The save button can be used for exporting the segmentation into an .sgm file. The user can load the segmentation and modify it later on using the load button on the left.

Once the segmentation is completed, it can be saved in an .sgm file. The format of the file is minimalistic; the first value in the file is an integer; stating the number of peaks in the file. The second value is also an integer, stating the number of float fields in each peak. In our application, each peak is described by four values: The first value is the location of the peak, in terms of milliseconds. The second is the width of the peak; which is used by some segmentation algorithms. The third feature is the amplitude of the peak. Finally, the fourth feature states the type of the peak ($S_1 = 0$, $S_2 = 1$). All these four features are written as float numbers to the .sgm with this order. The file format is extensible in the sense that the user might choose to save more features than 4 for each peak. As long as the first four features are not altered, all of the algorithms described in this paper would work without any problem. Users can export their segmentations to .sgm files using the Save button in the Segmentation category as shown in Figure 4.8

UpBeat also has a simple feature display tool, which finds the valid S_1 - S_2 - S_1 subchains in the segmentation, and draws these intervals by warping them such that the systolic periods will overlap. The average of the energies of all such available beats are then used for calculating 32 equidistant features, which are then shown in the feature display window. The feature display tool can be toggled using the eye icon as shown in Figure 4.9. This allows the user to intuit

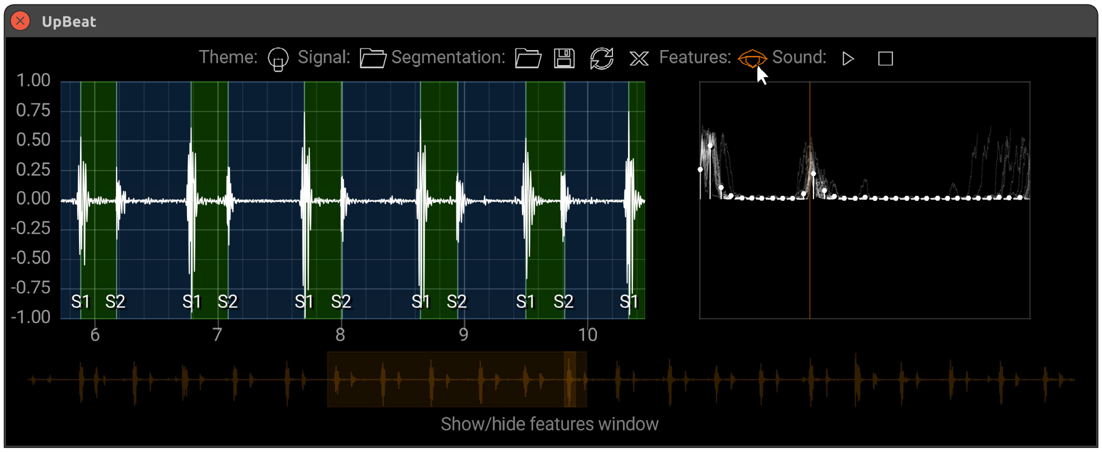

Figure 4.9: The feature display tool, which provides an intuition about the correctness of the segmentation.

how correct their segmentation process is. Any singular beat that is visibly off can be observed.

We have also implemented a "quick segmentation" method, where the annotator plays the sound and presses the Space key whenever they want to add a peak to the position of yellow progress bar (which indicates the position of the playback). If the previous peak is S_1, the following peak will be added as an S_2 and vice versa. Furthermore, each of these peaks will immediately snap to the closest largest sample in the data, so that they can properly show the positions of the peaks. This was an experimental inclusion for Prof. Dr. Ali Oto to use, and is not visible on the menu; however it remains fully functional.

UpBeat is capable of creating, loading, editing and saving a segmentation scheme using a set of helpful features, and is capable of calculating and displaying the average time-domain features of the cardiac cycle. Among the features of our program is the playback of the sound, automatic segmentation of the signal; easy-to-use interface for manual segmentation, and finally an advanced zoom mechanism that allows detailed analysis of portions to be segmented. The presented tool can be used to create a ground truth for heart sound segmentation. It is a starting medium for other researchers to expand on what is available.

Chapter 5

Implementation of the Heart Sound Segmentation Algorithms

As previously discussed, the majority of the work in the literature follows a pattern that can be separated into six sequential steps, and the variation between different PCG segmentation papers originate from their selection of methods in each of these six steps.

Comparison of these methods as they are given in the literature would be incomplete. An approach taken in Part 1 by Method X might have been very useful to be used with Method Y in Part 2. We compared every combination of all the methods discussed in Chapter 3, also including novel ideas in several steps. In total, we tested more than 240 variations. Naturally, not all of these combinations are meaningful, as to be seen empirically.

5.1 Algorithms

We have implemented several algorithms, including a majority of the work in the literature. At several steps, we have our own contributions. We also implemented other approaches such as MMR.

5.1.1 The Generic 6-Step Algorithm

The steps of the 6-step approach described in the related work are implemented as follows.

5.1.1.1 Preprocessing

All the inputs of the program are re-sampled to a frequency of 4410 Hz, and then normalized, such that the amplitude of the signal is scaled between -1 and 1. It has been shown that this works better than the statistical normalization in our case [23].

5.1.1.2 Time-frequency Transform

For the time-frequency transform step; STFT, Constant Q-transform, Daubechies-4 wavelet and band pass filter are implemented. The FFT size for the STFT scheme is set to 256, where the window function is selected as

$$w[n] = \frac{1 - cos(2\pi n/256)}{2}$$

For the D4 wavelet, we consider d7, d6, d5 and a5 bands; which correspond to the frequency bands 34.45 - 68.90 Hz, 68.90 - 137.81 Hz, 137.81 - 275.63 Hz, and 0 - 137.81 Hz, respectively. Hedayioglu and Liang et al. use d4, d5 and a4 bands; which correspond to the 138 - 275 Hz, 69 - 138 Hz and 0-138 Hz bands with their sampling frequency [6, 29].

Our contributions in this step are the Constant Q-transform and the band-pass filter. The band-pass filter is designed to pass frequencies between 30 Hz and 60 Hz, using MATLAB's *fdatool*. Since some approaches only considered the 45 Hz band for segmentation; filtering the 30-60 Hz band makes sense.

Constant-Q transform was implemented as described by Brown [45]. Short-time approach for time-frequency analysis is implemented, also the output is modified to return the absolute value instead of complex output. We divide the 32 - 64 Hz band into 8 bins, therefore $Q = 1/(2^{(1/8)} - 1) \approx 11$. We empirically found out that these parameters provide a sharp representation of S_1 and S_2 sounds.

5.1.1.3 Rectification and Envelope Detection

Absolute value, energy, Shannon energy and Shannon entropy are implemented as is. Since envelogram and homomorphic filter provide very similar results, only envelogram is implemented.

5.1.1.4 Thresholding and Merging Peaks

Both methodologies proposed by Gupta et al. and Hedayioglu [6, 23] are implemented. The approach that Liang et al. proposed is very similar to that of Hedayioglu, the only difference is the peak classification. We implemented our own peak classification method that outperform these.

At each step, we also consider the case where that step is omitted. The total number of combinations is 240; as depicted in Figure 5.1.

5.1.2 MMR

We have also proposed another approach that does not follow the regular algorithmic framework. The idea behind this approach is that we want to find the highest peaks in the rectified signal, assuming that these peaks represent the S_1 and S_2 sounds (Note that the regular threshold method also makes the assumption that these sounds have high amplitudes).

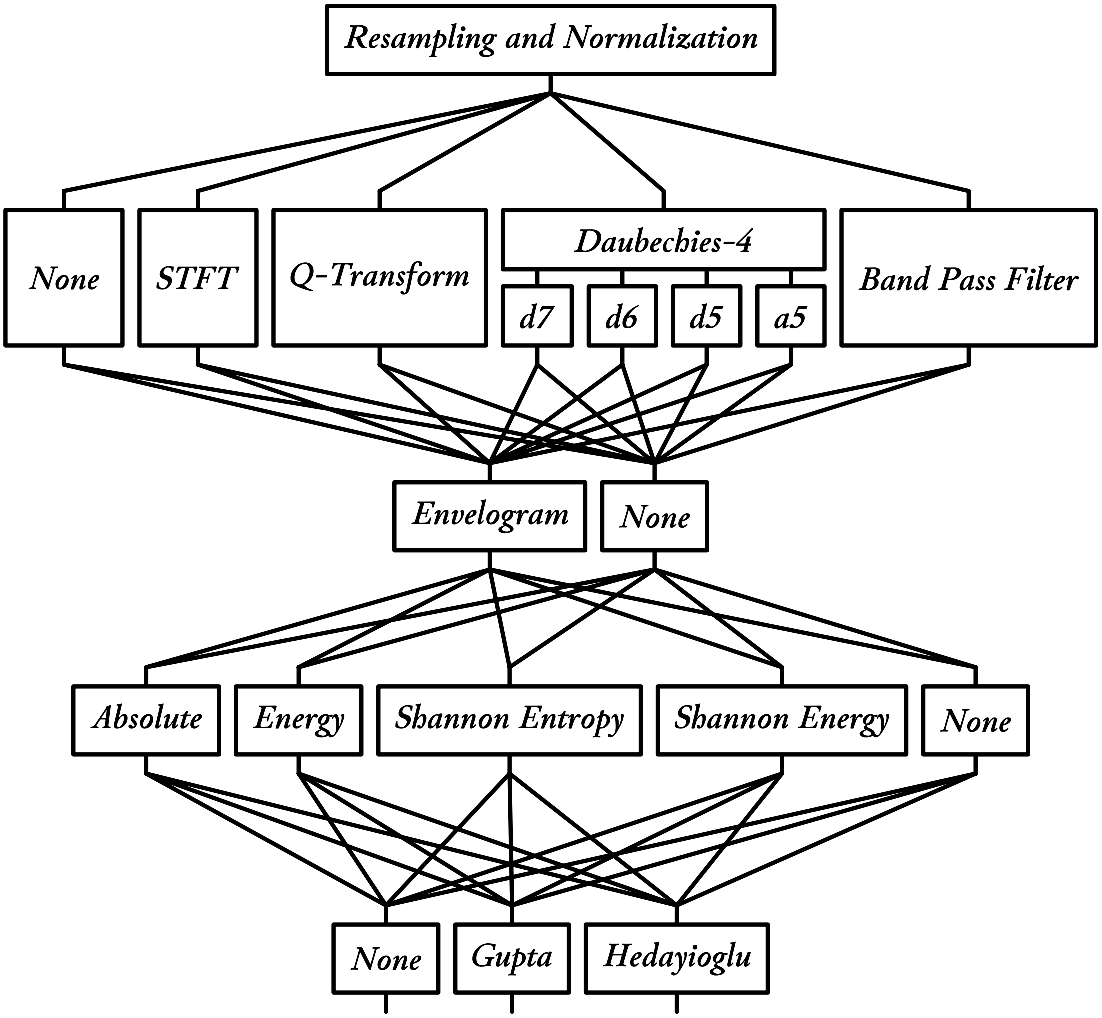

Figure 5.1: Every variation of the generic 6-step algorithm. There are 240 possibilities, some of which might be redundant.

If each peak consisted of only one sample that is high, this could have been achieved by *sorting* the samples and taking the highest peaks. However, if n^th sample has the highest amplitude, it is very probable that the second highest sample will become either $n-1$ or $n+1$. Therefore we also want this ranking to be *diverse*, such that every peak is represented in the highest samples list with a single point. Diversity means that the peaks are temporally separated in this context.

In order to achieve diversity, we employ the MMR equation proposed by Carbonell et al. [33] as below:

$$MMR = \arg \max_{D_i \in R \setminus S} \left[\lambda Sim_1(D_i, Q) - (1-\lambda) \max_{D_j \in S} Sim_2(D_i, D_j) \right]$$

This equation was proposed for text retrieval, however we can convert it to fit our needs. For example, we can define each *document* D_i as the samples from the signal, (t_i, y_i). Let Q be a constant value such that $y_i \leq Q$ for any i. We select $Q = \max_{D_i \in S} y_i$. Then the L-distance to query is defined as $dist(D_i, Q) = |Q - y_i|/Q = 1 - y_i/Q$. If the signal is normalized beforehand, then $Q = 1$ is a simple choice; in which case $Sim_1(D_i, Q) = y_i$.

We also want the retrieved peaks to be diverse in terms of their positions in time. However we need this metric to be normalized as well. We selected the Gaussian probability distribution as below:

$$Sim_2(D_i, D_j) = \frac{1}{\sqrt{2\pi\sigma}} e^{-\frac{(D_i - D_j)^2}{2\sigma^2}}.$$

The parameter σ gives us a non-linear elasticity on the importance of the distance of peaks. We can set this parameter to highly discourage any other samples within the range of a peak.

The MMR formula is altered as follows:

$$\begin{aligned} MMR &= \arg \max_{D_i \in D \setminus S} \left[\lambda y_i - (1-\lambda) \max_{D_j \in S} \frac{1}{\sqrt{2\pi\sigma}} e^{-\frac{(D_i - D_j)^2}{2\sigma^2}} \right] \\ &= \arg \max_{D_i \in D \setminus S} \left[\lambda y_i - \frac{1-\lambda}{\sqrt{2\pi\sigma}} e^{-\frac{\min_{D_j \in S} (D_i - D_j)^2}{2\sigma^2}} \right] \end{aligned}$$

Given that both similarity metrics were normalized between 0 and 1, ranking is not affected by amplitude scaling and duration of the signal.

Since the data points are considered as discrete independent documents, this method also does not assume equidistant sampling. Therefore one can optimize the MMR process by reducing samples. For example, samples below a low threshold (e.g. the median of the signal) can be removed. Instead, we used an elimination process where the taken samples are supposed to be the local maxima in their 1-neighborhood, similar to how 1D SIFT algorithm detects key points [50].

MMR is an iterative process; therefore requires the number of peaks to be detected (k). Also, λ should be specified in advance. We added an extra parameter called Δ. The iterations are continued as long as there is at least one interval greater than Δ, or the number of added peaks is less than k. Using 2-fold cross-validation, we detected that $\lambda = 0.5$, $\sigma = 120$ ms, $\Delta = 375$ ms, $k = t_N/200$ ms are optimal. This is meaningful biologically, since 120 ms is the widest a peak can be [23]; and $2k = 400$ ms is a feasible mean length for periods.

Chapter 6

Evaluation and Conclusion

6.1 Dataset

In order to test our methods, we used the Pascal heart sound classification challenge dataset [1].

Pascal dataset consists of two subsets, called Dataset A and Dataset B. Dataset A is classified into four subcategories named ‘normal’, ‘murmur’, ‘extra heart sound’ and ‘artifact’; whereas Dataset B consists of three classes named as ‘normal’, ‘murmur’ and ‘extrasystole’. Although the total number of recordings in the dataset is 862; only the recordings in the ‘normal’ category has segmentation information for us to use as ground truth during evaluation. We have also eliminated two segmentation schemes, because they had typos in the file that corresponded to invalid segmentation schemes. Finally, any file with a duration less than 2 seconds has been discarded, since most of the methods to be compared require at least a few beats so that statistical parameters make sense. In the end we are left with 66 reliable files.

6.2 Evaluation

All methods listed in the previous chapter are tested on the reduced dataset. Although there are evaluation techniques proposed in the literature, most of these metrics do not handle the case where the numbers of detected peaks to not match. For instance, below is the evaluation metric required by the Pascal challenge [1]:

$$\delta_k = \frac{\sum_{i=1}^{N_k/2} (|RS1_i - TS1_i| + |RS2_i - TS2_i|)}{N_k}$$

where δ_k is the average distance of the k^{th} recording in the dataset, N_k is the total number of peaks in the ground truth, $RS1_i$ ($RS2_i$) are the locations of S_1 (S_2) peaks of the i^th heartbeat in the ground truth, $TS1_i$ ($TS2_i$) are the locations of S_1 (S_2) peaks in the calculated segmentation. The total error of the algorithm on the entire dataset of N documents is calculated as

$$\delta = \sum_{j=0}^{N} \delta_j.$$

The assumption inherent in this scheme is that all peaks in the ground truth have corresponding peaks in the calculated segmentation. This may not be the case if several peaks are missed (Type-II error), or if extra peaks are included (Type-I error). One implementation would be to match the closest peak of the same type for every peak; however in that case making a Type-I error has no cost (since there will be no extra peaks to match these peaks), whereas Type-II errors will have a distance longer than a beat can be. This is also not desired, because a missing peak might not be a big problem for the classification algorithm that will follow. Reversing the order in which we check the integrity of the peaks does not help either. Below are several evaluation metrics we propose.

6.2.1 Method 1

We have proposed a more strict evaluation approach as follows. For every S_1-S_2-S_1 sub-chain ('beat') in the ground truth segmentation, let the temporal locations of these peaks be t_{i-1}, t_i and t_{i+1}. The calculated segmentation scheme is said to have this beat if and only if all the following conditions hold:

1. There exists exactly one S_1 peak t'_{i-1} within the range $[t_{i-1} - \tau, t_{i-1} + \tau]$.
2. There exists **no** S_2 peaks within this range.
3. There exists exactly one S_1 peak t'_{i+1} within the range $[t_{i+1} - \tau, t_{i+1} + \tau]$.
4. There exists **no** S_2 peaks within this range.
5. There exists exactly one S_2 peak t'_i within the range $[t'_{i-1}, t'_{i+1}]$.
6. There exists **no** S_1 peaks within this range.

If all of these conditions are satisfied, the beat is said to have been detected by the algorithm. The number of the detected beats is then divided to the number of beats in the ground truth, which gives us an accuracy score, where the greater value is better. Our tests revealed that $\tau = 50$ ms provides a distinguishing ranking, which also makes sense since a peak may have a width of 100 ms. An example to how these rules work is depicted in Figure 6.1.

6.2.2 Method 2

Although the first evaluation method we propose is more to-the-point in that it directly evaluates the ratio of cardiac cycles we correctly annotate; the discrete nature of it requires another more sensitive evaluation metric. For example, consider two segmentation algorithms. For each ground truth peak p_i at $t = t_i$, let the first algorithm A_1 annotate a peak at $t = t_i + 30$ ms, and the second algorithm A_2 annotate a peak at $t = t_i - 4$ ms. Assume the type of peak (S_1/S_2)

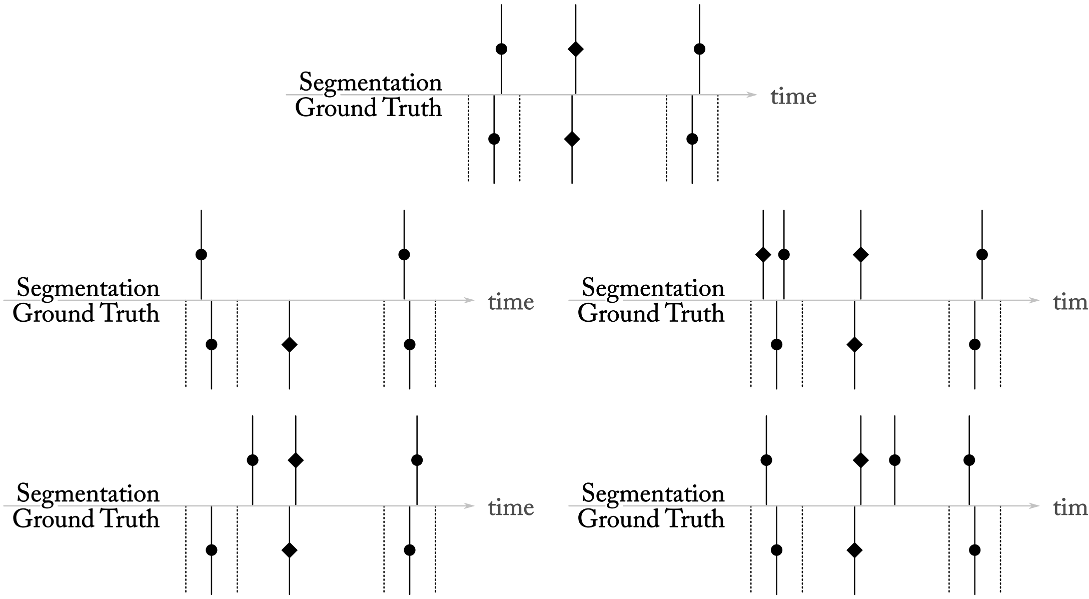

Figure 6.1: Several cases which involves the first evaluation metric. S_1 peaks are described with lines with circles on them, and S_2 lines have diamonds. The dashed lines represent the τ neighborhood of the S_1 peaks. Of all the cases above, only the first (topmost) is considered a valid (detected) beat.

is correct for all peaks in both A_1 and A_2. Since both algorithms generate unique peaks within the 50 ms range of the ground truth, both will have a score of 1.0. However, in reality A_2 consistently produces closer results to the ground truth. It can be argued that the first metric fails to differentiate between these two cases. For this purpose we suggest a second evaluation metric as follows.

Since the intervals between an S_1 and the following S_2 is a systolic period, and the interval between an S_2 and the following S_1 peak is a diastolic, and these two regions never overlap; one can separate the time domain of a heart sound signal into two subsets as S and D, respectively. The time domain is separated by the ground truth into two such subsets as S_G and D_G, whereas the same time domain is divided into S_C and D_C by the calculated peaks. If these regions perfectly overlap, then segmentation is 100% successful.

Let $SS = |S_G \cap S_C|$, $DD = |D_G \cap D_C|$, $SD = |S_G \cap D_C|$, and $DS = |D_G \cap S_C|$. These four parameters represent the cardinalities (in this case, *total lengths*) of regions, respectively, in which:

1. Both the ground truth and solution are in systolic region,
2. Both the ground truth and solution are in diastolic region,
3. The ground truth is in the systolic region, but the solution claims diastolic region,
4. The ground truth is in the diastolic region, but the solution claims systolic region.

Whereas SS and DD are correct classifications, SD and DS are incorrect. Therefore a metric can be defined as $x = \frac{SS+DD}{SS+DD+SD+DS}$. When the ground truth and calculated segmentations are identical, $x = 1$. However, the implication of the case where $x = 0$ is that $SS = DD = 0$. This means that the segmentation locations are still identical, however every systolic period is identified as a diastolic and vice versa. Therefore this is similar to correlation, in that a random (uncorrelated) segmentation would yield $x = 0.5$ instead of 0. Therefore we update our evaluation metric as

$$|2x - 1| = |2\frac{SS + DD}{SS + DD + SD + DS} - 1| = |\frac{SS + DD - SD - DS}{SS + DD + SD + DS}|.$$

This version will yield 1 when the segmentations are identical, and 0 when completely uncorrelated. An example is seen in Figure 6.2.

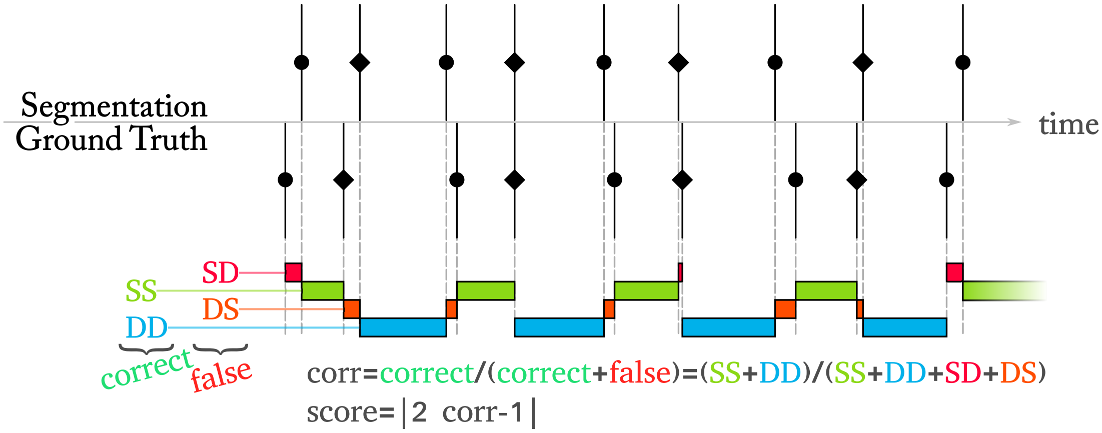

Figure 6.2: An example of how the second evaluation metric is calculated. S_1 peaks are described with lines with circles on them, and S_2 lines have diamonds.

6.2.3 Method 3

We have also developed a third metric that makes use of the Hungarian algorithm to assign calculated peaks to the ground truth peaks. For n ground truth peaks and m calculated peaks; we construct an $n \times m$ distance matrix M, such that m_{ij} has the distance between i^{th} ground truth peak and j^{th} calculated peak (that is, $m_{ij} = t_i - t'_j$). Then we try to assign ground truth peaks and calculated peaks to each other, such that the total distance is minimized. This means that we are trying to assign every calculated peak to the closest ground truth peak; and this corresponds to picking $min\{n, m\}$ elements from M that minimizes their total with the condition that at most one element is selected from every row and column. This is an NP-complete problem and can be solved using the Hungarian algorithm. The summation can then be divided by the number of peaks to provide a score. Unlike the two previous scores, in Method 3 the smaller score is better.

However, there are some problems with this approach. The fact that in the ground truth dataset the annotations are not 'snapped' to the maximum samples of each peak, but rather is placed at the beginning of each peak, means that the best algorithm might not have the smallest error. Over-optimizing the similarity in this fashion might be (and as we will see in the Results section, *is*) erroneous.

6.3 Results

The methods listed in Chapter 5 are tested on a valid subset of the Pascal heart sound challenge dataset [1]. There were 66 normal heart sound recordings in Dataset A and Dataset B combined with a valid annotation, full segmentation and a duration longer than 3 seconds. This limitation on the file duration is required since most of the methods do not work on very short files, which consist of very few segments. Also, several files were not completely segmented, which would mean that the evaluation quality would be reduced due to an erroneous ground truth dataset. Such files were also excluded. Finally, annotations of two heart sound files had errors. Excluding all these files, we ended up with a reliable dataset of 66 sound files.

We have tested all the algorithm variations on all files. For each algorithm, we calculate the evaluation scores and average them over these 66 files. We repeated these tests for all of our evaluation metrics. Results are listed below, with respect to each evaluation metric.

6.3.1 Metric 1

Step 1	Step 2	Step 3	Step 4&5	Score
None	Envelogram	Energy	Gupta	0.62660
MMR				0.61779
QTransform	None	Absolute	None	0.61691
QTransform	None	None	None	0.61691
QTransform	None	Absolute	Gupta	0.59621
QTransform	None	None	Gupta	0.59621
QTransform	Envelogram	Absolute	None	0.59503
QTransform	Envelogram	None	None	0.59503
QTransform	None	ShannonEnergy	Gupta	0.58386
BandPassFilter	Envelogram	Energy	Gupta	0.58241
QTransform	Envelogram	Absolute	Gupta	0.57699
QTransform	Envelogram	None	Gupta	0.57699
BandPassFilter	Envelogram	ShannonEnergy	Gupta	0.57544
DaubechiesD4_D5Band	Envelogram	Energy	Gupta	0.56933
STFT	Envelogram	Absolute	Gupta	0.56634
STFT	Envelogram	None	Gupta	0.56634
QTransform	Envelogram	ShannonEnergy	Gupta	0.56158
STFT	Envelogram	Energy	Gupta	0.55962
STFT	Envelogram	Energy	None	0.55461
DaubechiesD4_A5Band	Envelogram	Energy	Gupta	0.55354

Table 6.1: Evaluation scores of the top-20 algorithms, according to Evaluation Metric 1

Table 6.1 lists the scores of the top 20 algorithms, according to our first evaluation metric. Maximal Marginal Relevance outperforms all methods except Gupta's method with no initial time-frequency transform. This might be because the signals in the datasets are already preprocessed. Q-Transform and band pass filter appear to be competing with the methods in the literature. Also, since our implementation of Q-Transform reduces the number of samples taken (due to high computational cost), envelogram becomes a redundant step.

6.3.2 Metric 2

Table 6.2 lists the scores of the top 20 algorithms with respect to our second evaluation metric. Maximal Marginal Relevance outperforms all other methods. The following four methods are also the Top-4 results for the first metric. Again, Q-Transform without envelogram produces competitive results.

Step 1	Step 2	Step 3	Step 4&5	Score
	MMR			0.62383
None	Envelogram	Energy	Gupta	0.61765
QTransform	None	Absolute	None	0.58738
QTransform	None	None	None	0.58738
BandPassFilter	Envelogram	ShannonEnergy	Gupta	0.58497
BandPassFilter	Envelogram	Energy	Gupta	0.57260
QTransform	None	ShannonEnergy	Gupta	0.57005
None	Envelogram	ShannonEnergy	Gupta	0.56909
QTransform	Envelogram	Absolute	None	0.56585
QTransform	Envelogram	None	None	0.56585
DaubechiesD4_A5Band	Envelogram	Energy	Gupta	0.56577
QTransform	None	Absolute	Gupta	0.56332
QTransform	None	None	Gupta	0.56332
STFT	Envelogram	Energy	Gupta	0.54927
STFT	Envelogram	Absolute	Gupta	0.54921
STFT	Envelogram	None	Gupta	0.54921
QTransform	Envelogram	Absolute	Gupta	0.54908
QTransform	Envelogram	None	Gupta	0.54908
BandPassFilter	Envelogram	Absolute	Gupta	0.54320
STFT	Envelogram	Energy	None	0.54087

Table 6.2: Evaluation scores of the top-20 algorithms, according to Evaluation Metric 2

6.3.3 Metric 3

Table 6.3 lists the scores of the top 20 algorithms with respect to our second evaluation metric. Unlike the previous two metrics, these results do not appear to be informative; as the first 86 algorithms have an average error below 50 ms. Also, because the peaks in the ground truth seem to be annotated at the beginning of the peak instead of at the largest sample, the exact average distance to the peaks might not be a very sensitive measure. Although the MMR method does not appear in this list, its average error is 35.32 ms, giving it a 52^{nd} order.

Step 1	Step 2	Step 3	Step 4&5	Score
DaubechiesD4_D6Band	Envelogram	Absolute	Hedayioglu	13.36058
STFT	Envelogram	Energy	Hedayioglu	14.00491
STFT	Envelogram	Absolute	Hedayioglu	14.74057
STFT	Envelogram	None	Hedayioglu	14.74057
DaubechiesD4_D6Band	Envelogram	ShannonEnergy	Hedayioglu	15.90085
DaubechiesD4_D6Band	Envelogram	Energy	Hedayioglu	17.9021
QTransform	None	Energy	Hedayioglu	18.02057
DaubechiesD4_D5Band	Envelogram	ShannonEnergy	Hedayioglu	20.25292
DaubechiesD4_A5Band	Envelogram	Energy	Hedayioglu	20.26519
DaubechiesD4_D5Band	Envelogram	Absolute	Hedayioglu	20.27933
QTransform	None	Absolute	Hedayioglu	21.10549
QTransform	None	None	Hedayioglu	21.10549
DaubechiesD4_A5Band	Envelogram	Absolute	Hedayioglu	21.24261
QTransform	Envelogram	Energy	Hedayioglu	22.03681
STFT	Envelogram	ShannonEnergy	Hedayioglu	22.64943
BandPassFilter	Envelogram	Absolute	Hedayioglu	22.68577
QTransform	None	Energy	Gupta	24.02679
DaubechiesD4_D5Band	Envelogram	None	Hedayioglu	24.08979
BandPassFilter	Envelogram	Energy	Gupta	24.21508
None	Envelogram	Absolute	Hedayioglu	24.43124

Table 6.3: Evaluation scores of the top-20 algorithms, according to Evaluation Metric 3

We also attempted to create an ensemble of methods in order to increase the scores further.

6.4 Ensemble

Although we have a ranking of methods, the scores obtained do not have statistically significant advantage over each other. In order to achieve better performance, we propose an ensemble of 24 methods. Table 6.4 lists the methods that we picked for this ensemble.

We first calculated that if we had a perfect ensemble metric, such that for each file we could perfectly select the best performing algorithm we have; then the ensemble score would be 0.84 (according to the first evaluation score). This means that although singular methods cannot exceed a score of 0.63, this is not an upper limit enforced by the dataset, and there is significant room for improvement.

We attempted to use the standard deviation of the systolic and diastolic intervals as an ensemble score, however this further reduces the ensemble score. Our final metric is as follows:

To merge the methods, we count the number of S_1 - S_2 - S_1 chains in the calculated segmentation, and divide it to the total number of peaks. The segmentation scheme with a higher ratio of such chains has a higher score. Whichever algorithm has the highest score for a given file is selected as the answer, and presented as the outcome of the ensemble. Our ensemble achieved a score of 0.75123, outperforming any singular method. The same ensemble has an evaluation score of 0.77259 according to the second metric.

The ensemble has a score of 37.460518 ms according to the third evaluation metric, which is ‘worse’ than the top-20 methods. This strengthens our concerns regarding the inefficiency of the third metric.

Step 1	Step 2	Step 3	Step 4&5
STFT	Envelogram	Absolute	Gupta
QTransform	Envelogram	Absolute	Gupta
DaubechiesD4_D6Band	Envelogram	Absolute	Gupta
DaubechiesD4_D5Band	Envelogram	Absolute	Gupta
DaubechiesD4_A5Band	Envelogram	Absolute	Gupta
BandPassFilter	Envelogram	Absolute	Gupta
None	Envelogram	Absolute	Gupta
STFT	Envelogram	Energy	Gupta
DaubechiesD4_D6Band	Envelogram	Energy	Gupta
DaubechiesD4_D5Band	Envelogram	Energy	Gupta
BandPassFilter	Envelogram	Energy	Gupta
None	Envelogram	Energy	Gupta
BandPassFilter	Envelogram	ShannonEntropy	Gupta
DaubechiesD4_D6Band	Envelogram	ShannonEnergy	Gupta
BandPassFilter	Envelogram	ShannonEnergy	Gupta
DaubechiesD4_D5Band	Envelogram	None	Gupta
STFT	None	Absolute	Gupta
None	Envelogram	Absolute	Hedayioglu
STFT	Envelogram	ShannonEntropy	Hedayioglu
DaubechiesD4_D6Band	Envelogram	ShannonEntropy	Hedayioglu
DaubechiesD4_A5Band	Envelogram	ShannonEnergy	Hedayioglu
STFT	None	ShannonEnergy	Hedayioglu
None	Envelogram	Energy	None
MMR			

Table 6.4: Methods selected for the ensemble

6.5 Conclusion

In this work we have investigated the topic of heart sound segmentation. The literature on cardiac analysis lacks the unification of results on a common data set with properly defined evaluation metrics. We have implemented, compared and combined the majority of the work in the literature. We have also proposed several additions on the generic 6-step segmentation algorithm, as well as introducing the well-known Maximal Marginal Relevance equation on the segmentation problem. We introduced two evaluation measures which take into consideration the Type-I and Type-II errors that can occur on segmentation. When tested with the first evaluation metric, the maximal marginal relevance method outperforms other algorithms, whereas the Constant-Q transform competes with other methods effectively. We also described a way of combining several methods in order to increase performance. While the maximum score a singular method could achieve was 0.63 (meaning that the 63 percent of heartbeats have been correctly annotated with at most a 50 ms deviation from the ground truth), our ensemble shows 0.75 accuracy. The second evaluation metric that we introduce provides a similar ranking for the methods that we evaluate. In this case, the maximum score belongs to the MMR algorithm (0.62), whereas the ensemble has a score of 0.77.

We also programmed an intuitive, easy-to-use standalone application that can be used for manual heart sound segmentation to allow constructing ground truth datasets, or provide a means of visualization that can help obtain an insight on the heart sound waveform. The tests were performed on the 66 suitable files in Pascal dataset. We propose as future work to extend the dataset for more reliable tests, refine the ensemble method as empirical results show that there is more room for performance improvement, and experiment with other time-frequency transform methods such as SAX [51] and piecewise linear modeling [52] etc.

Bibliography

[1] P. Bentley, G. Nordehn, M. Coimbra, and S. Mannor, “The PASCAL Classifying Heart Sounds Challenge 2011 (CHSC2011) Results.” http://www.peterjbentley.com/heartchallenge/index.html, 2011.

[2] D. Venes, *Taber’s cyclopedic medical dictionary.* FA Davis, 2013.

[3] “Cardiovascular System at the US National Library of Medicine Medical Subject Headings (MeSH).” `http://goo.gl/G4xLvg`, 2011.

[4] A. Alwan *et al.*, *Global status report on noncommunicable diseases 2010.* World Health Organization, 2011.

[5] World Health Organization, *Noncommunicable Diseases (NCD) Country Profiles.* 2014.

[6] F. d. L. Hedayioglu, “Heart sound segmentation for digital stethoscope integration,” 2011.

[7] “Heart murmur - wikipedia, the free encyclopedia.”

[8] OkCopay, “National median costs of MRI scans.” `http://www.okcopay.com/results/mri-abdominal`.

[9] T. T. Birliği, “Resmi sağlık kurumları fiyat tarifesi.” `http://www.ttb.org.tr/mevzuat/2005ek/but/EK-82.htm`, 2014.

[10] T. C. Lin, *Phonocardiogram segmentation.* PhD thesis, 2005.

[11] J. Vepa, "Classification of heart murmurs using cepstral features and support vector machines," in *Engineering in Medicine and Biology Society, 2009. EMBC 2009. Annual International Conference of the IEEE*, pp. 2539–2542, IEEE, 2009.

[12] S. Jabbari and H. Ghassemian, "Modeling of heart systolic murmurs based on multivariate matching pursuit for diagnosis of valvular disorders," *Computers in biology and medicine*, vol. 41, no. 9, pp. 802–811, 2011.

[13] E. Delgado-Trejos, A. Quiceno-Manrique, J. Godino-Llorente, M. Blanco-Velasco, and G. Castellanos-Dominguez, "Digital auscultation analysis for heart murmur detection," *Annals of biomedical engineering*, vol. 37, no. 2, pp. 337–353, 2009.

[14] C. G. DeGroff, S. Bhatikar, J. Hertzberg, R. Shandas, L. Valdes-Cruz, and R. L. Mahajan, "Artificial neural network–based method of screening heart murmurs in children," *Circulation*, vol. 103, no. 22, pp. 2711–2716, 2001.

[15] S. L. Strunic, F. Rios-Gutiérrez, R. Alba-Flores, G. Nordehn, and S. Burns, "Detection and classification of cardiac murmurs using segmentation techniques and artificial neural networks," in *Computational Intelligence and Data Mining, 2007. CIDM 2007. IEEE Symposium on*, pp. 397–404, IEEE, 2007.

[16] Z. Syed, D. Leeds, D. Curtis, F. Nesta, R. A. Levine, and J. Guttag, "A framework for the analysis of acoustical cardiac signals," *Biomedical Engineering, IEEE Transactions on*, vol. 54, no. 4, pp. 651–662, 2007.

[17] C. Ahlstrom, P. Hult, P. Rask, J.-E. Karlsson, E. Nylander, U. Dahlström, and P. Ask, "Feature extraction for systolic heart murmur classification," *Annals of biomedical engineering*, vol. 34, no. 11, pp. 1666–1677, 2006.

[18] F. Javed and P. Venkatachalam, "A signal processing module for the analysis of heart sounds and heart murmurs," in *Journal of Physics: Conference Series*, vol. 34, p. 1098, IOP Publishing, 2006.

[19] Y. Chen, S. Wang, C.-H. Shen, and F. K. Choy, "Matrix decomposition based feature extraction for murmur classification," *Medical engineering & physics*, vol. 34, no. 6, pp. 756–761, 2012.

[20] A. Quiceno-Manrique, J. Godino-Llorente, M. Blanco-Velasco, and G. Castellanos-Dominguez, "Selection of dynamic features based on time–frequency representations for heart murmur detection from phonocardiographic signals," *Annals of biomedical engineering*, vol. 38, no. 1, pp. 118–137, 2010.

[21] F. Wang, T. Syeda-Mahmood, and D. Beymer, "Finding disease similarity by combining ecg with heart auscultation sound," in *Computers in Cardiology, 2007*, pp. 261–264, IEEE, 2007.

[22] M. G. Johnson, A. Tewfik, K. Madhu, and A. G. Erdman, "Using voice-recognition technology to eliminate cardiac cycle segmentation in automated heart sound diagnosis," *Biomedical Instrumentation & Technology*, vol. 41, no. 2, pp. 157–166, 2007.

[23] C. N. Gupta, R. Palaniappan, S. Swaminathan, and S. M. Krishnan, "Neural network classification of homomorphic segmented heart sounds," *Applied Soft Computing*, vol. 7, no. 1, pp. 286–297, 2007.

[24] H. N. Liang *et al.*, "A feature extraction algorithm based on wavelet packet decomposition for heart sound signals," Time-Frequency and Time-Scale Analysis, 1998. Proceedings of the IEEE-SP International Symposium on, 1998.

[25] G. Livanos, N. Ranganathan, and J. Jiang, "Heart sound analysis using the s transform," in *Computers in Cardiology 2000*, pp. 587–590, IEEE, 2000.

[26] O. Abdel-Alim, N. Hamdy, and M. El-Hanjouri, "Heart diseases diagnosis using heart sounds," in *Radio Science Conference, 2002.(NRSC 2002). Proceedings of the Nineteenth National*, pp. 634–640, IEEE, 2002.

[27] M. W. Groch, J. R. Domnanovich, and W. D. Erwin, "A new heart-sounds gating device for medical imaging," *Biomedical Engineering, IEEE Transactions on*, vol. 39, no. 3, pp. 307–310, 1992.

[28] A. Haghighi-Mood and J. Torry, “A sub-band energy tracking algorithm for heart sound segmentation,” in *Computers in Cardiology 1995*, pp. 501–504, IEEE, 1995.

[29] H. Liang, S. Lukkarinen, and I. Hartimo, “Heart sound segmentation algorithm based on heart sound envelogram,” in *Computers in Cardiology 1997*, pp. 105–108, IEEE, 1997.

[30] A. C. Stasis, E. Loukis, S. Pavlopoulos, and D. Koutsouris, “Using decision tree algorithms as a basis for a heart sound diagnosis decision support system,” in *Information Technology Applications in Biomedicine, 2003. 4th International IEEE EMBS Special Topic Conference on*, pp. 354–357, IEEE, 2003.

[31] S. Choi and Z. Jiang, “Comparison of envelope extraction algorithms for cardiac sound signal segmentation,” *Expert Systems with Applications*, vol. 34, no. 2, pp. 1056–1069, 2008.

[32] A. Mondal, P. Bhattacharya, and G. Saha, “An automated tool for localization of heart sound components s1, s2, s3 and s4 in pulmonary sounds using hilbert transform and heron’s formula,” *SpringerPlus*, vol. 2, no. 1, pp. 1–14, 2013.

[33] J. Carbonell and J. Goldstein, “The use of mmr, diversity-based reranking for reordering documents and producing summaries,” in *Proceedings of the 21st annual international ACM SIGIR conference on Research and development in information retrieval*, pp. 335–336, ACM, 1998.

[34] S. K. Mitra and Y. Kuo, *Digital signal processing: a computer-based approach*, vol. 2. McGraw-Hill New York, 2006.

[35] A. E. Cetin, “Lecture notes on discrete-time signal processing.” `http://kilyos.ee.bilkent.edu.tr/~ee424/EE424.pdf`, 2012. [Online; accessed 7-May-2015].

[36] J. Allen, “Short term spectral analysis, synthesis, and modification by discrete fourier transform,” *Acoustics, Speech and Signal Processing, IEEE Transactions on*, vol. 25, pp. 235–238, Jun 1977.

[37] C. K. Chui, *An introduction to wavelets*, vol. 1. Academic press, 2014.

[38] I. Daubechies *et al.*, *Ten lectures on wavelets*, vol. 61. SIAM, 1992.

[39] L. Chun-Lin, "A tutorial of the wavelet transform," *NTUEE, Taiwan*, 2010.

[40] R. G. Stockwell, L. Mansinha, and R. Lowe, "Localization of the complex spectrum: the s transform," *Signal Processing, IEEE Transactions on*, vol. 44, no. 4, pp. 998–1001, 1996.

[41] R. A. Brown and R. Frayne, "A fast discrete s-transform for biomedical signal processing," in *Engineering in Medicine and Biology Society, 2008. EMBS 2008. 30th Annual International Conference of the IEEE*, pp. 2586–2589, IEEE, 2008.

[42] S. Mallat, *A wavelet tour of signal processing.* Academic press, 1999.

[43] A. Alhazred, "The Necronomicon (Al Azif)."

[44] J. C. Brown and M. S. Puckette, "An efficient algorithm for the calculation of a constant q transform," *The Journal of the Acoustical Society of America*, vol. 92, no. 5, pp. 2698–2701, 1992.

[45] J. C. Brown, "Calculation of a constant q spectral transform," *The Journal of the Acoustical Society of America*, vol. 89, no. 1, pp. 425–434, 1991.

[46] N. Baddour, "Heart Signal Recordings - Invitro and Invivo," 04 2014.

[47] A. Gharehbaghi, T. Dutoit, A. Sepehri, P. Hult, and P. Ask, "An automatic tool for pediatric heart sounds segmentation," in *Computing in Cardiology, 2011*, pp. 37–40, IEEE, 2011.

[48] E. F. Gomes, A. M. Jorge, and P. J. Azevedo, "Classifying heart sounds using multiresolution time series motifs: an exploratory study," in *Proceedings of the International C* Conference on Computer Science and Software Engineering*, pp. 23–30, ACM, 2013.

[49] A. Castro, T. T. Vinhoza, S. S. Mattos, and M. T. Coimbra, “Heart sound segmentation of pediatric auscultations using wavelet analysis,” in *Engineering in Medicine and Biology Society (EMBC), 2013 35th Annual International Conference of the IEEE*, pp. 3909–3912, IEEE, 2013.

[50] D. G. Lowe, “Distinctive image features from scale-invariant keypoints,” *International journal of computer vision*, vol. 60, no. 2, pp. 91–110, 2004.

[51] J. Lin, E. Keogh, S. Lonardi, and B. Chiu, “A symbolic representation of time series, with implications for streaming algorithms,” in *Proceedings of the 8th ACM SIGMOD workshop on Research issues in data mining and knowledge discovery*, pp. 2–11, ACM, 2003.

[52] M. Johansson, “Piecewise linear modeling,” in *Piecewise Linear Control Systems*, pp. 9–31, Springer, 2003.